THE UNIVERSITY OF MICHIGAN

4386-2-F

AFCRL 62-91

AN INVESTIGATION OF THE ABSORPTION OF ELECTROMAGNETIC RADIATION BY A PLASMA OF SUB-CRITICAL DENSITY

Final Report

by

A. Olte, M. L. Barasch, E. G. Fontheim, A. E. Heins
J. S. King and E. K. Miller

February 1962

The work described in this report was supported by
the ADVANCED RESEARCH PROJECTS AGENCY,
ARPA Order Nr. 187-61, Project Code 7200,
Contract AF 19(604)-8032

prepared for

Electronics Research Directorate
Air Force Cambridge Research Laboratories
Office of Aerospace Research
Laurence G. Hanscom Field
Bedford, Massachusetts

Requests for additional copies by Agencies of the Department of Defense, their contractors, and other Government agencies should be directed to:

ARMED SERVICES TECHNICAL INFORMATION AGENCY
ARLINGTON HALL STATION
ARLINGTON 12, VIRGINIA

Department of Defense contractors must be established for ASTIA services or have their "need-to-know" certified by the cognizant military agency of their project or contract.

All other persons and organizations should apply to:

U. S. DEPARTMENT OF COMMERCE
OFFICE OF TECHNICAL SERVICES
WASHINGTON 25, D. C.

TABLE OF CONTENTS

ABSTRACT

The design of an experiment is given which employs an inverted coaxial diode geometry to investigate absorption of electromagnetic radiation below and above the plasma frequency. Data obtained when a pure electron stream is introduced into the system are analyzed, but cannot be completely explained. Difficulties encountered in introducing and ionizing a real gas are discussed.

The results of an investigation concerning the form of the electron distribution function in such an experimental arrangement are reported.

Finally, the process of free-free absorption is discussed, and expressions are given for the absorption coefficient in the presence of ions and neutral atoms or molecules. These are shown to be essentially equivalent to the results of the usual Lorentzian theory.

I
INTRODUCTION

This report is a continuation of a study (Goodrich, et al 1960) initiated two years ago to investigate experimentally and theoretically the absorption of electromagnetic waves by a plasma. The paramount necessity to account fully for alternative explanations of the communications blackouts, both re-entry and thermonuclear, was the primary motivation of the work.

The evident lack of sufficient experimental results to check and verify the existing plasma theories over an adequate range of parameters led to a simple and well-defined plasma experiment. An inverted co-axial diode was designed and built as an integral part of a broadband co-axial microwave transmission line. Microwave attenuation data was to be obtained for a pure electron stream and for an ionized gas case to check and verify the existing plasma theories.

An independent theoretical study was carried out to examine alternative and possibly new absorption mechanisms of electromagnetic waves in a plasma. This led to a consideration of the free-free absorption at frequencies exceeding the plasma frequency. The free-free absorption was the only significant mechanism found to be operative, or indeed even expected. A thorough quantum statistical formulation of this process was initiated and completed successfully.

From these statements, it is clear that the work reported here divides naturally into three aspects. The first of these is the experimental investigation

which includes the design of the experiment, the results obtained in the laboratory, and the discussion of these results in terms of the Lorentzian plasma. We have not been able so far to account for the absorption effects in a pure electron stream either in terms of a simple equivalent Lorentzian model or by some other method. Due to some experimental difficulties the absorption data so far obtained on the ionized gas is inadequate for presentation and analysis. The second chapter is a theoretical effort to obtain the electron density distribution functions in the tube for an ionized gas. This function is of cardinal importance in interpreting the experimental electromagnetic wave absorption effects. The third chapter is a theoretical investigation of the free-free absorption. Formulas for the absorption coefficients are presented and discussed. The conclusion reached, however, is that this process is simply an alternative description of the usual process of collisional loss, agreeing with the predictions of accepted theory in their region of joint validity.

II
A COAXIAL LOW-DENSITY PLASMA EXPERIMENT

2.1 Introduction

The scattering of electromagnetic radiation by ionized gases with densities below 10^{13} ions per cm^3 is of general interest in the communication field. Detailed experimental data in the vicinity of the plasma frequency is of particular interest in revealing the importance of possible interaction mechanisms and the validity of some commonly used formulas describing the electromagnetic wave interaction with plasmas.

Measurements of the interaction of microwaves with gas discharges have been numerous since the early experiments of Tonks (1931). Romell (1951), examined the differential scattering from a 3.2cm diameter plasma column placed between two yagi antennas. Herschberger (1960) extended the experiments of Romell (1951) and Dattner (1957), using a 0.5cm diameter discharge tube placed across a 3.0in x 1.5in. rectangular waveguide, and between open waveguide ends. The response to variable plasma densities was observed at a fixed signal frequency of 2800 Mc. Golant et al (1961) have obtained data from the positive column of a hot cathode gas discharge in glass bulbs axially inserted in a cylindrical waveguide.

Interpretation of these and similar experiments are complicated by the boundary conditions around the plasma and by the sensitivity of the results on the

microwave structure near the plasma. Furthermore, they are fixed frequency measurements in which the functional dependence on the microwave frequency cannot be directly observed.

The present experiment was undertaken with three purposes in mind; first, to produce an interaction in a simpler geometry, i.e., one approaching the ideal of a free space plane wave incident on a plane uniform ionized gas barrier; second, to observe the interaction as a continuous function of signal frequency, and third, to initially test the interpretability of this arrangement with the simplest plasma, i.e., a collision-free electron cloud whose density and distribution should be accurately predicted. It is believed that the first two purposes have largely been achieved by the apparatus described below. The use of an electron cloud, however, has not necessarily produced an ideal plasma, because electron-conductor wall collisions have replaced gas collisions. Extension of the measurements to ionized gases is a natural second step.

The construction of the apparatus was finished during the first quarter. The second quarter was spent in shakedown experiments and some modification of the cathode heater assembly. At the beginning of the third quarter a cathode of 14cm length (nominal) was successfully activated. Extensive reflection and transmission measurements were made on this diode without any gas present. Upon conclusion of these experiments, first nitrogen and then helium gas was

introduced into the system. A rather strong cathode poisoning resulted and no useful results were obtained. The purity of the gases was questioned, but was found to be adequate. When the gas was introduced into the vacuum envelope at a pressure of 1mm of Hg, it was necessary, of course, to turn off the 140 liter ionization pump. Sufficient amounts of 'dirty' gas then evolved from the system itself to poison the oxide cathode. This was discouraging. However, it was discovered that the adsorption type fore-pumps when chilled to liquid nitrogen temperature did not pump helium to any significant extent. Thus these pumps could be used to keep the helium atmosphere clean for a sufficient length of time to conduct the experiment. By this time however, the 14cm cathode was poisoned beyond recovery. A new cathode was inserted for activation at the beginning of the last quarter. While activating this cathode an arc developed from cathode to anode, and the anode was punctured releasing cooling water, so that it was necessary to replace the cathode, the anode, and one ceramic plate. As a result the new 20.3 cm cathode was activated only two weeks before the end of the fourth and last quarter. The pure electron results were repeated, but there was no time left to carry on the helium ionization experiments.

The apparatus is described in some detail in Section 2.2. The measurements on the two cathodes and the analysis of the data is given in Section 2.3.

2.2 Experimental Design

The experimental apparatus is essentially a rigid 50 ohm transmission line with a wide band RF generator at one end and suitable detector and load termination at the other end. A central 15 in. section of this line is a removable coaxial diode which is operated in a high vacuum by looping the line through a 36 in. deep by 18 in. diameter vacuum manifold. The diode produces an electron plasma region with a length (d) to annular width (r_c-r_a) ratio of about 100. The complete line is shown in the scaled drawing of Figure 2.1. The physical arrangement of the components around the vacuum console is shown in Figure 2.2. In the diode section the cathode forms the outer conductor and the anode the inner conductor of the coaxial line, in contrast to the usual arrangement. Thermionic emission is produced by radiant heating of the outer conductor surface by a tungsten wire heater surrounded by a platinum reflector. Anode heat from the electron bombardment is carried away by water flow inside the anode conductor. The water flow is dead-ended and thus requires only one exit path from the transmission line. As shown in Figure 2.1, this exit path is through an adjustable shorted quarter-wave line to eliminate reflections.

The coaxial line was designed to minimize reflections and losses everywhere in the absence of the ion cloud. Except for short external connecting cables the line is a rigid structure, mostly of nickel tubing, with the central conductor

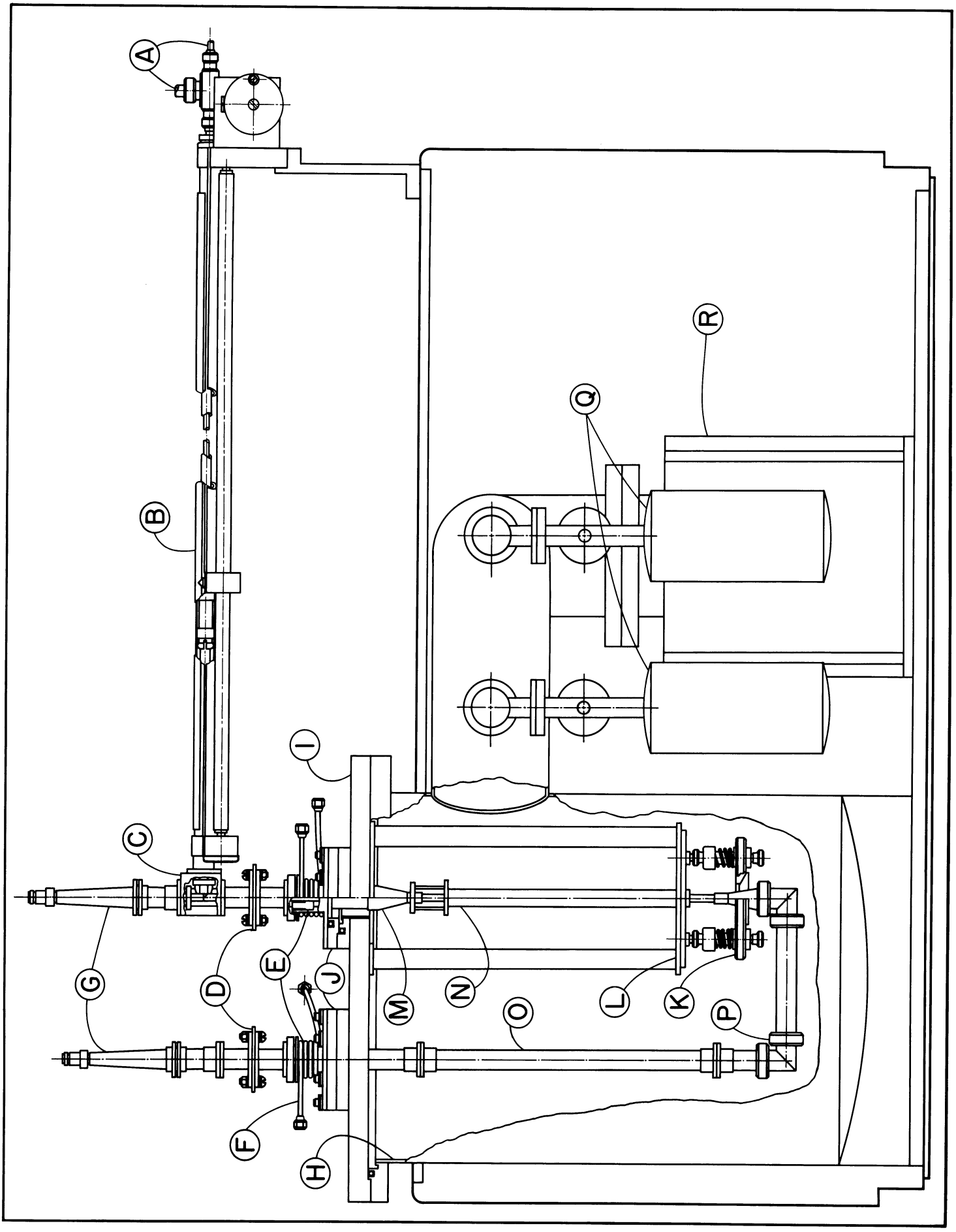

FIGURE 2.1: SCHEMATIC OF THE EXPERIMENT

LEGEND FOR FIGURE 2.1

A	Concentric Coolant Tube Entrance and Exit
B	Quarter Wave Shorting Stub
C	Shorting Stub Split Tee Block
D	DC Isolation Capacitors
E	Teflon Vacuum Tight Support Beads
F	Support Bead Cooling Coil
G	Tapered Transitions to Input and Output Coaxial Cables
H	Vacuum Tank
I	Vacuum Tank Cover Place
J	DC Insulated Vacuum Flanges
K	Diode Centering and Tension Plate
L	Tension Plate Assembly
M	Tapered Transitions to Coaxial Diode
N	Coaxial Diode, Heater Windings and Heat Reflector
O	Return Path Coaxial Line
P	Quartz Support Bead Housing
Q	"Vacsorb" Forepumps
R	"Vacion" High Vacuum Pump

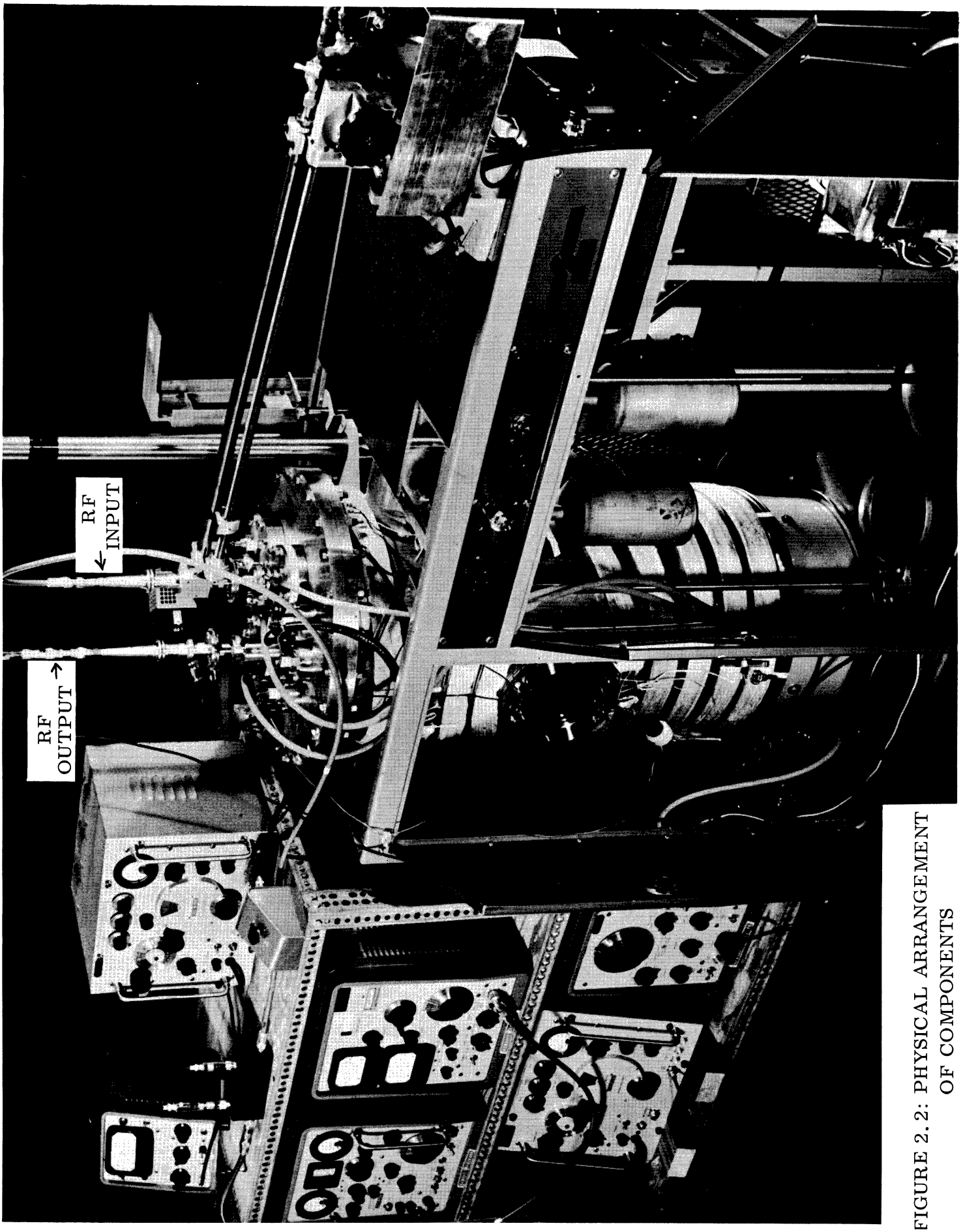

FIGURE 2.2: PHYSICAL ARRANGEMENT OF COMPONENTS

supported by a minimum number of insulating beads. Gradually tapered ends are used at the two external terminals and at the diode ends. DC isolation of the negative potential cathode is achieved by two large series capacitors of high dielectric constant.

The long, smooth coaxial geometry offers several key advantages to the analysis of the experiment:

(a) the waveguide can be made to propagate only the simplest wave, the transverse electromagnetic mode (TEM),

(b) "unclean" boundary conditions at the extremities of the plasma region become insignificant with a large length-to-width ratio,

and

(c) the waveguide has a very broad band response which permits variation of the transmitted RF frequency, f, around any fixed plasma frequency f_p. While the reverse operation is also possible, enough uncertainty exists in the exact determination of the plasma frequency that f_p is better used as a parameter than a variable.

There are, also, practical difficulties in the design:

(a) the primary difficulty is the construction of the long, narrow diode whose anode must be coaxially symmetric yet unsupported, small in diameter yet capable of high power dissipation, and whose cathode requires a long internal oxide coated surface, not obtainable from commercial tube manufacturers,

and

(b) the cathode is a 'one-shot' device and the diode is unavailable for adjustment once the cathode is activated inside the vacuum system.

The Coaxial Diode. The details of the diode design are shown in Figure 2.3. The anode passes through a teflon vacuum seal above the vacuum cover plate, tapers to a small radius in the active cathode region and joins the central conductor below a second taper. The bottom tip is threaded into a retention nut inside the inner conductor. Tightening this nut applies the centering and tensioning action of the anode stretcher assembly shown in Figure 2.1. The cathode is a nickel tube 15.75 in. long, with an inside diameter of 0.356 in. and a wall thickness of 0.012 in., which makes a sliding fit into the ends of the two heavy nickel taper sections. A 12 in. longitudinal tungsten filament heater is mounted on ceramic insulators which are positioned inside the cylindrical platinum heat shield. A difference in thermal expansion of the cathode over the anode of up to 0.15 in. is allowed by the sliding joints, which, however, do not impair electrical continuity.

Selection of the outer conductor as the cathode was made to optimize the radial uniformity of the electron density distribution. If ρ is the electron density, r_c the cathode radius, and I_o the diode current per unit length, the cylindrical form of Child's law for space charge limited operation can be written as an expansion in r

$$\rho(r) = -\left(\frac{\epsilon_o m}{18\pi^2 e}\right)^{1/3} \frac{I_o^{2/3}}{r^{4/3}\beta^{2/3}} \qquad (2\text{-}1)$$

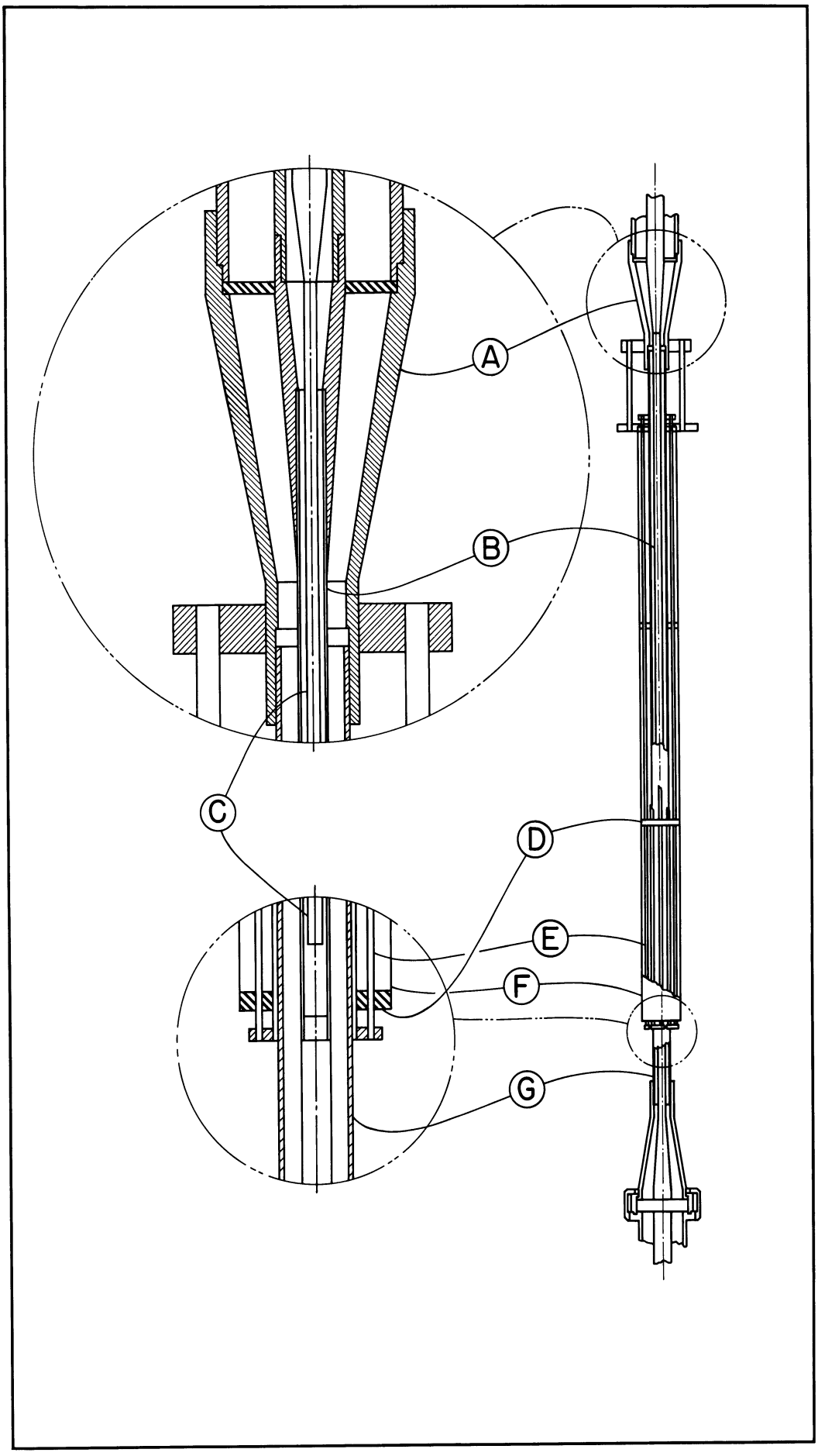

FIGURE 2.3: DETAILS OF DIODE DESIGN

LEGEND FOR FIGURE 2.3
(All dimensions in inches)

A	Tapered Transition to Coaxial Diode
B	Anode and Outer Coolant Tube .156 Outside Dia. .136 Inside Dia.
C	Inner Coolant Tube .093 Outside Dia. .085 Inside Dia.
D	Ceramic Guide and Spacers for Heater Rods
E	Tungsten Heater Rods .030 Dia. Twelve Rods Equally Spaced Around Cathode on .600 Dia. Rode Circle
F	Platinum Heater Reflector .800 Outside Dia. .790 Inside Dia. 12.437 Long
G	Nickel Cathode .380 Outside Dia. .356 Inside Dia. 15.750 Long

where the function β both for the regular and the inverted diode was obtained by Langmuir and Bldogett (1923); ϵ_o, m and e are the permittivity of free space (MKS), the electronic mass, and charge. The density function is quite different depending on whether r is greater or less than r_c. Figure 2.4 is a plot of $\rho(r)$ versus r/r_c and r_c/r for the normal and inverted diodes respectively. Both functions go to infinity at $r=r_c$ but the inverted diode has a minimum point and reverses slope. Hence, selection of the anode radius such that r_c/r is about 3.0 or less, results in a reasonably uniform density over all but the outer radii, in contrast with the normal case. The ratio used in the present experiment is 2.28. Since the plasma frequency depends on the half-power of $\rho(r)$ we conclude that the variation of f_p around its average is less than 8 percent over 60 percent of the plasma area as compared to 50 percent variation over this same area in the normal diode. Furthermore, the influence of the spike in $\rho(r)$ near the cathode is less important, in the inverted case, in determining the effective average dielectric constant for the plasma.

The radial dimensions should be as large as possible for adequate coolant area and for precision of annular spacing. They are, however, severely limited by power requirements. The companion equation to (2-1) relating voltage and charge density is

$$V(r) = -\frac{\rho(r)}{\epsilon_o}\,\frac{9}{4}\,r^2\beta^2 \quad . \qquad (2\text{-}2)$$

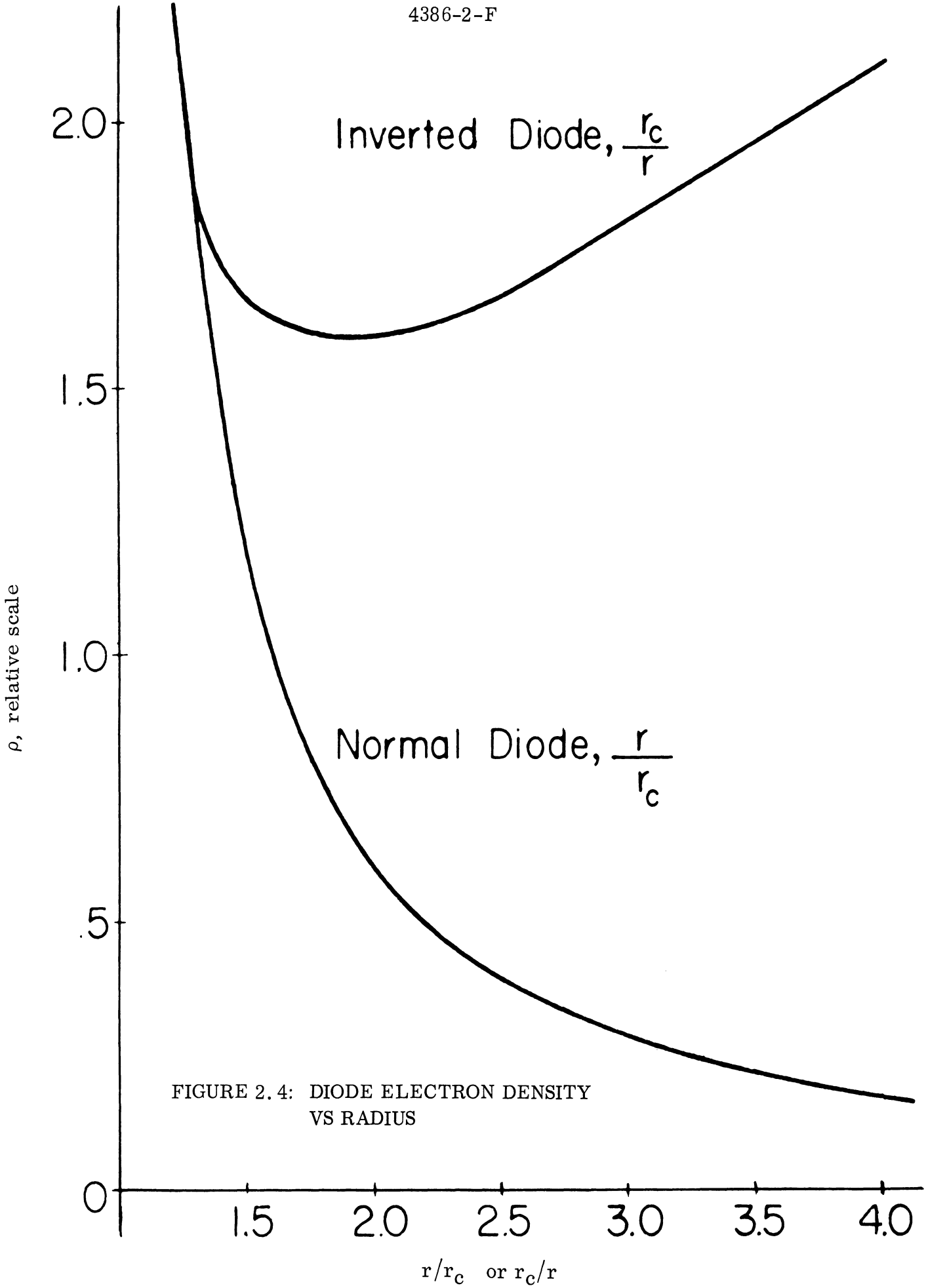

FIGURE 2.4: DIODE ELECTRON DENSITY VS RADIUS

Hence the plate power per unit length is, from (2-1) and (2-2),

$$V(r_a) I_o = \left[\left(\frac{9}{2\epsilon_o}\right)\left(\frac{\pi^2 e}{m}\right)\right]^{1/2} r_a^4 \cdot \rho(r_a)^{5/2} \cdot \beta^3 \quad . \qquad (2\text{-}3)$$

The ratio r_a/r_c is approximately fixed by the need for density uniformity, and the value of ρ at $r=r_a$ is typical of the annular region average. Hence, (2-3) displays the strong dependence of power on r_a and ρ average. There is evidently a need to minimize r_a to reach the highest possible ρ . The first diode was constructed with the values,

$$r_c/r_a = 2.28, \text{ and } \quad r_a = 0.078 \text{ in.}$$

A safe upper bound for heat flux across the anode wall is about 100 watts/cm^2. For this limit and the above radii, (2-3) gives the electron density at the anode $\rho(r_a) \approx 1.6 \times 10^9/\text{cm}^3$.

It is not reasonable to push the electron density much above 2.0×10^9 since this would require the radii to be unusably small and high pressure cooling would be necessary. Electron densities near or above $10^{10}/\text{cm}^3$ can only be reached by pulsed operation of the diode plate voltage. This has not been attempted as yet.

The axial length of the diode must be long to provide enough plasma length to produce clearly measurable changes in the reflection and transmission coefficients, Γ and τ, in the vicinity of the plasma frequency. The anode cannot be bead supported in and near the active cathode region, however, because of

sputtering from the cathode. Hence the anode length between closest bead supports should be small for mechanical rigidity. A compromise is therefore necessary in the choice of length. The effect of plasma length, d, on τ and Γ can be demonstrated by considering the simplest possible model of interaction, namely, the passage of the principal coaxial mode (TEM) through a uniform electron cloud in which no electron collisions occur, either with gas molecules or container walls. The equation of motion for the electrons gives the well-known disperson relation

$$k=k_o\left(1-\frac{f_p^2}{f^2}\right)^{1/2} \tag{2-4}$$

where the propagation vectors inside and outside the electron cloud are, respectively, $k=2\pi f\sqrt{\mu_o\epsilon}$ and $k_o=2\pi f\sqrt{\mu_o\epsilon_o}$. The plasma frequency

$$f_p=\left[\frac{N\,e^2}{4\pi^2\epsilon_o\,m}\right]^{1/2} \tag{2-5}$$

where N is the number of electrons per m^3. The electron cloud is in effect a dielectric region with specific capacity $K=(k/k_o)^2=\epsilon/\epsilon_o$. Use of the appropriate boundary conditions for incident, reflected, and transmitted plane waves leads to expressions for τ and Γ in terms of the plasma length, d. These are

$$\tau = \frac{4\sqrt{K}\;e^{ik_od}}{(1+\sqrt{K})^2\,e^{ikd}-(1-\sqrt{K})^2\,e^{-ikd}} \tag{2-6a}$$

and

$$\Gamma = \frac{(1-K)(e^{ikd}-e^{-ikd})}{(1+\sqrt{K})^2 e^{ikd}-(1-\sqrt{K})^2 e^{-ikd}} \quad . \tag{2-6b}$$

When the medium is lossless, we must have $|\Gamma| = \sqrt{1-|\tau|^2}$ in order to conserve energy. If the effect of elastic collisions is taken into account by including the usual Lorentz damping term in the equation of motion, the dispersion relation is modified by the inclusion of a collision frequency, ν, and equation (2-4) becomes

$$k=k_o \left[1-\frac{f_p^2}{f(f-i\frac{\nu}{2\pi})}\right]^{1/2} \quad . \tag{2-7}$$

Figure 2.5 is a plot of $|\tau|^2$ from (2-6a) for several plasma lengths d expressed in fractions of the plasma wavelength ($\lambda_p = c/f_p$). The solid curves correspond to $\nu = 0$ and the dotted curves show the effect of including a particular collision frequency. The effect of the actual non-uniformity in the electron distribution is discussed Section 2.3. Since some frequency-dependent fluctuation will occur in the measurements due to line reflections, the minimum desirable length should evidently not be less than about $\frac{1}{4}\lambda_p$. The heater length used for the present diode is 31.5cm and due to the axial temperature profile, this restricts the active region to about 23cm. This corresponds to a wavelength of 92cm or a plasma frequency of 326 Mc and a density ρ of 1.3×10^9 electrons/cm^3. Since this is near the density limit noted above, we conclude that the span of electron plasma frequencies available for good data is restricted to the region 100 to 400 Mc.

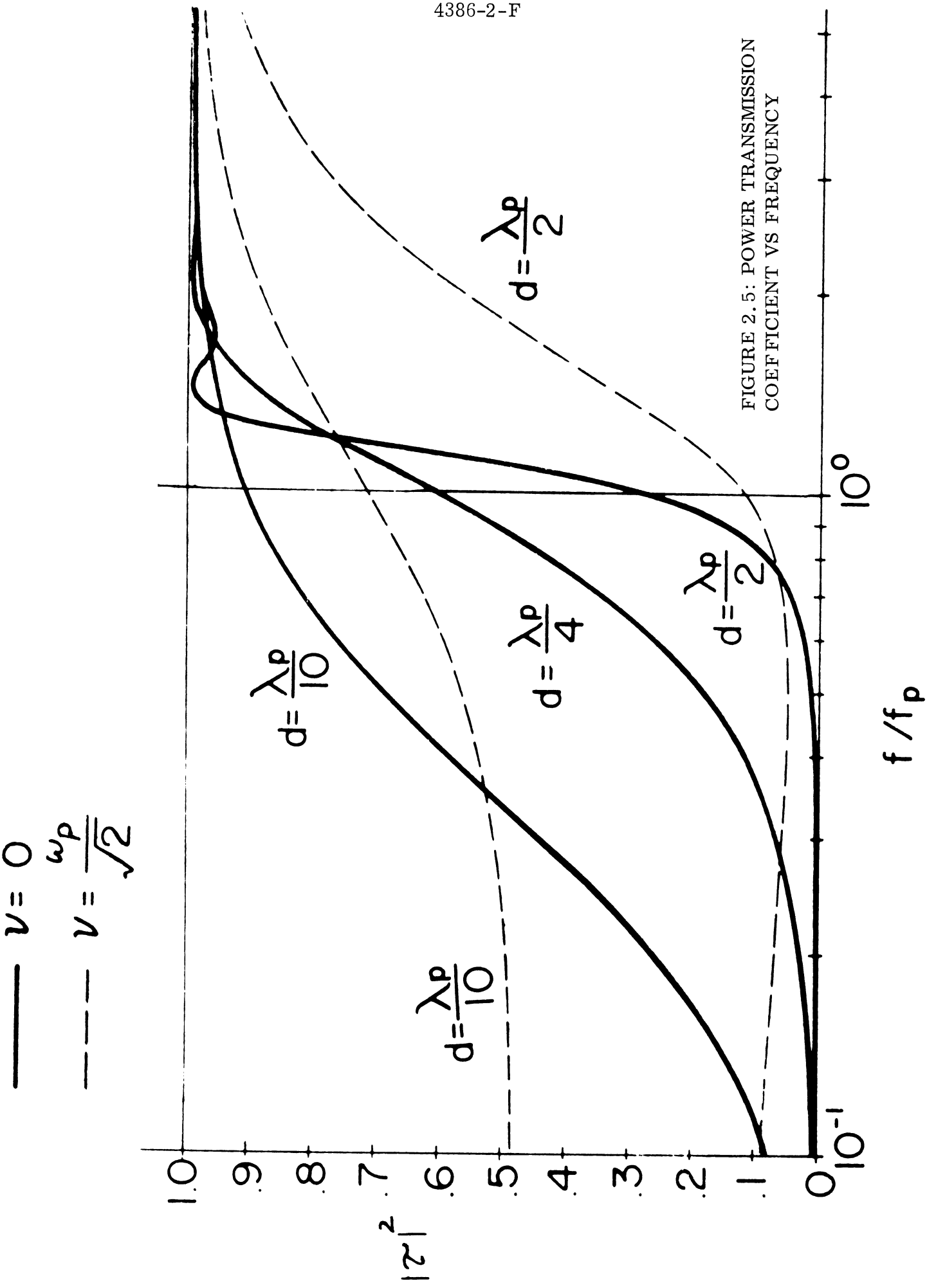

FIGURE 2.5: POWER TRANSMISSION COEFFICIENT VS FREQUENCY

The composition and activation of the cathode oxide surface followed normal procedures recommended by tube manufacturers. An unusual problem was encountered in coating the long, inside surface. Ba CO_2 and Sr CO_2 (Sylvania C10 triple carbonate) in a nitrocellulose lacquer and amyl acetate binder was applied as a liquid coating on this surface by the cathophoretic process. A technique of spin-drying was developed to promote a uniform depth of coating. The coated cathode was then mounted in the vacuum system and activated by heating from the diode heater. Difficulties in determining the actual pressure and temperatures at the cathode surface as well as an axial temperature gradient were encountered; the technique is still in a formative stage. However, two cathodes have been successfully developed.

The Anode Cooling System. The single-ended water cooling channel was designed to operate at an available tap pressure of 50 p.s.i. For a heat flux of 100 watts/cm^2 and the diode geometry already described, this corresponds to a bulk temperature rise of 30.3^{o}C and a heat dissipation of 3160 watts. Local boiling temperatures should not yet be reached according to conventional film drop calculation. Operation of electrically heated test models suggest, however, that local boiling does commence near 1500 watts input and the region of instable film boiling is reached above 2500 watts. Consequently, an upper limit of 2400 watts has so far been imposed on the diode operation. This corresponds, by

equation (2-3), to an electron density of 1.43×10^9 rather than the anticipated density of 1.6×10^9. The discrepancy in heat transfer properties is not yet understood and, because of inadequate test models, may not actually exist in the electron diode. The exceedingly small dimensions for the stainless steel tubing, shown in Figure 2.3, make support brackets for the inner tube impractical and consequently lack of concentricity is unavoidable. This may provide an explanation for the discrepancy.

Coaxial Support Beads. The center conductor of the coaxial loop is supported by ten dielectric beads each of which presents a dielectric discontinuity and hence a possible reflection. These reflections have been effectively compensated in the low frequency region below 3000 Mc by adjustment of the bead radial dimensions. The six beads, shown in Figure 2.1, inside the vacuum system are subjected to temperatures up to $200^{\circ}C$. Consequently, quartz (K=4.1) was used in this region. The rest of the beads are made of teflon.

The large teflon beads have a three-fold design requirement and were selected after considerable exploration. They must provide good RF impedance matching, mechanical strength against accidental vibrations, and a tension force of up to 100 pounds. They must also insure a high vacuum seal. The beads were surface etched to provide a bonding surface. A vacuum-tight bond to the nickel coaxial walls was achieved by .010 in. thick coating of epoxy resin. Metal and

teflon walls were scored 0.002 in. deep to promote bonding and the epoxy was built up on successive applications to seal against bubble leaks. External cooling coils insure that the teflon temperatures remain below 100°C . Operating experience with these beads has been quite satisfactory.

Vacuum System. The vacuum system was designed to provide a vacuum below 10^{-7}mm Hg which is sufficient for the protection of the activated cathode. The vacuum console was engineered by Varian Associates; most of the components are visible in Figure 2.2. The 150 liter test chamber is evacuated through a 5 in. manifold by two valved "Vacsorb" adsorption pumps and a "Vacion" ion pump. A Phillips-Granville controlled leak valve also connects to the manifold. All test penetrations into the system are made through the removable cover plate by means of several removable port flanges. These penetrations, all insulated, include the two coaxial seals, six thermocouple leads, and five heater and diode current leads. The test chamber walls can be preheated to 90°C for outgassing and are water-cooled during operation. Starting pressures are indicated by a thermocouple vacuum gauge and high vacua by the ion pump current directly. The ion pump has a flat pump rate characteristics of 140 liters/sec for air; the pump rate varies with the kind of gas being pumped.

Operating experience has shown that when the chamber is outgassed and without the diode heater on, indicated pressures of 4×10^{-8} mm Hg are normally

obtained, and this can be accomplished from open tank conditions in about 12 hours. With the heater on, the level rises to as high as 4×10^{-7} mm Hg. These pressures are believed to be quite satisfactory for a replaceable cathode. Longitudinal slits in the connecting tapered sections provide the pumping orifice. Thus there is some uncertainty, due to the closed nature of the diode design of the actual pressure in the diode during activation outgassing. This has hampered the activation operations.

RF System. The microwave detection is accomplished with conventional apparatus. Figure 2.6 is a typical arrangement used for measuring both transmitted and reflected power relative to input power. If the reflections from the coaxial line without electrons is small, the measurement of the transmission coefficient is especially simple: $|\tau|$ is just the ratio of transmitted voltage amplitudes for the heated electron tube with plate voltage on relative to plate voltage off. An alternative method for measuring reflected power utilizes a slotted line in place of the directional coupler and the VSWR is found with plate voltage on and off. In the reflection case, losses in the cable and the tube must be accounted for. The performance of the line and necessary corrections to the data are discussed in Section 2.3.

2.3. Experimental Results and Analyses

In the schematic of the experiment (Figure 2.1), the RF input and output

lines are shown enetering the vacuum console through the cover plate. The block diagram of the microwave circuit is shown in Figure 2.6. The power reflection and transmission coefficients of the circuit between the input and the output reference planes are shown in Figure 2.7. This measurement is carried out with the cathode hot but with no DC voltage on the diode. The reflections in the loop are small from 100 to 1000 Mc, moderate from 1000 to 3000 Mc, and unsatisfactorily large from 3000 to 4000 Mc. The power transmission coefficient varies from 0.9 at 200 Mc to 0.6 at 2000 Mc; in general it is decreasing with increasing frequency.

This variation is due primarily to the wall losses of the coaxial line. From the behavior of the transmission and the reflection parameters one may conclude that the microwave structure of Figure 2.1 may be represented by lossy transmission lines connecting the diode to the input and the output reference planes, as shown in Figure 2.6. This is a sufficiently good approximation for frequencies from 100 to 3000 Mc. For such a circuit the power transmission coefficient of the diode is readily obtained by monitoring the power at the output terminal with the cathode at the proper temperature and the DC voltage on the diode alternately on and off. The ratio of the power output with the DC voltage on, to that with the voltage off, is then the power transmission coefficient for that section of the coaxial line which contains the electrons.

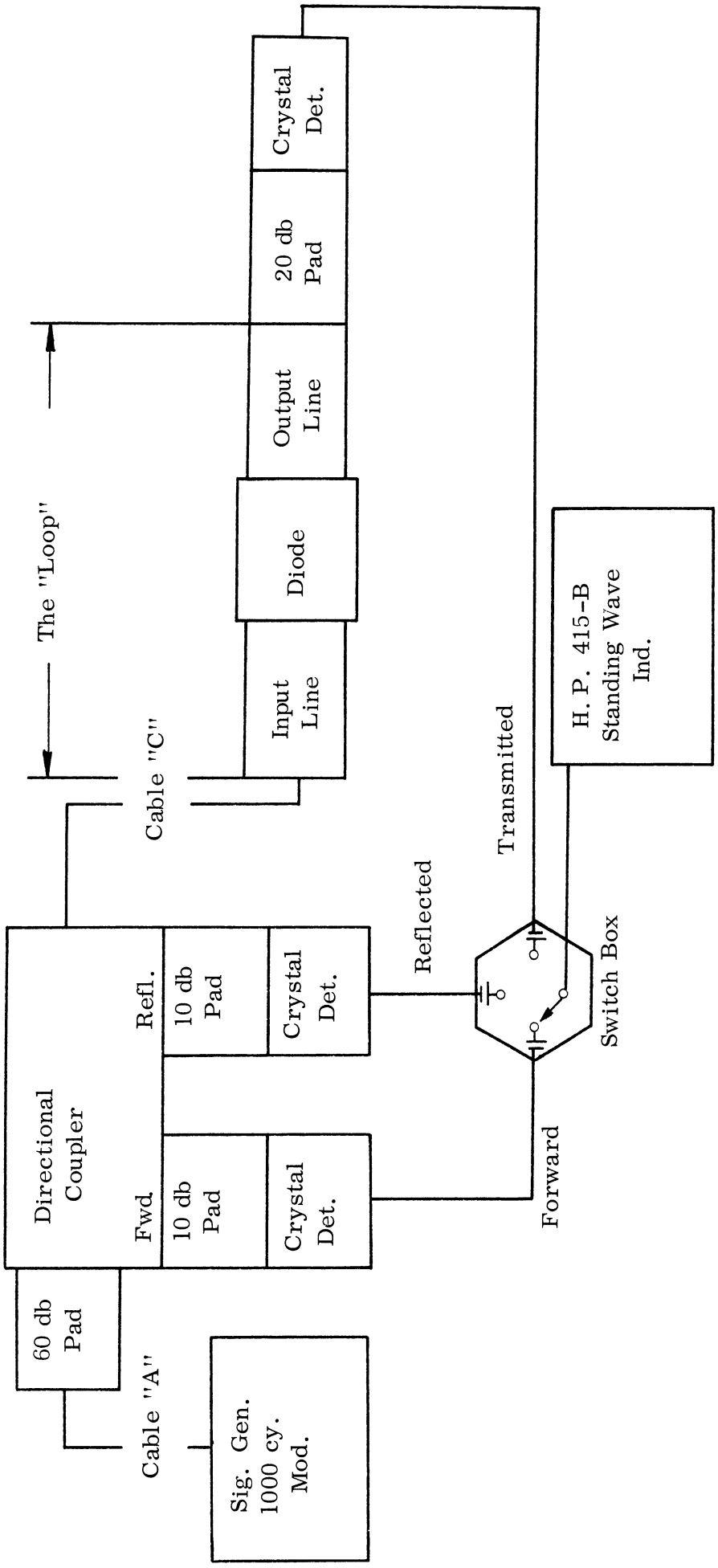

FIGURE 2.6: TYPICAL DETECTION SYSTEM

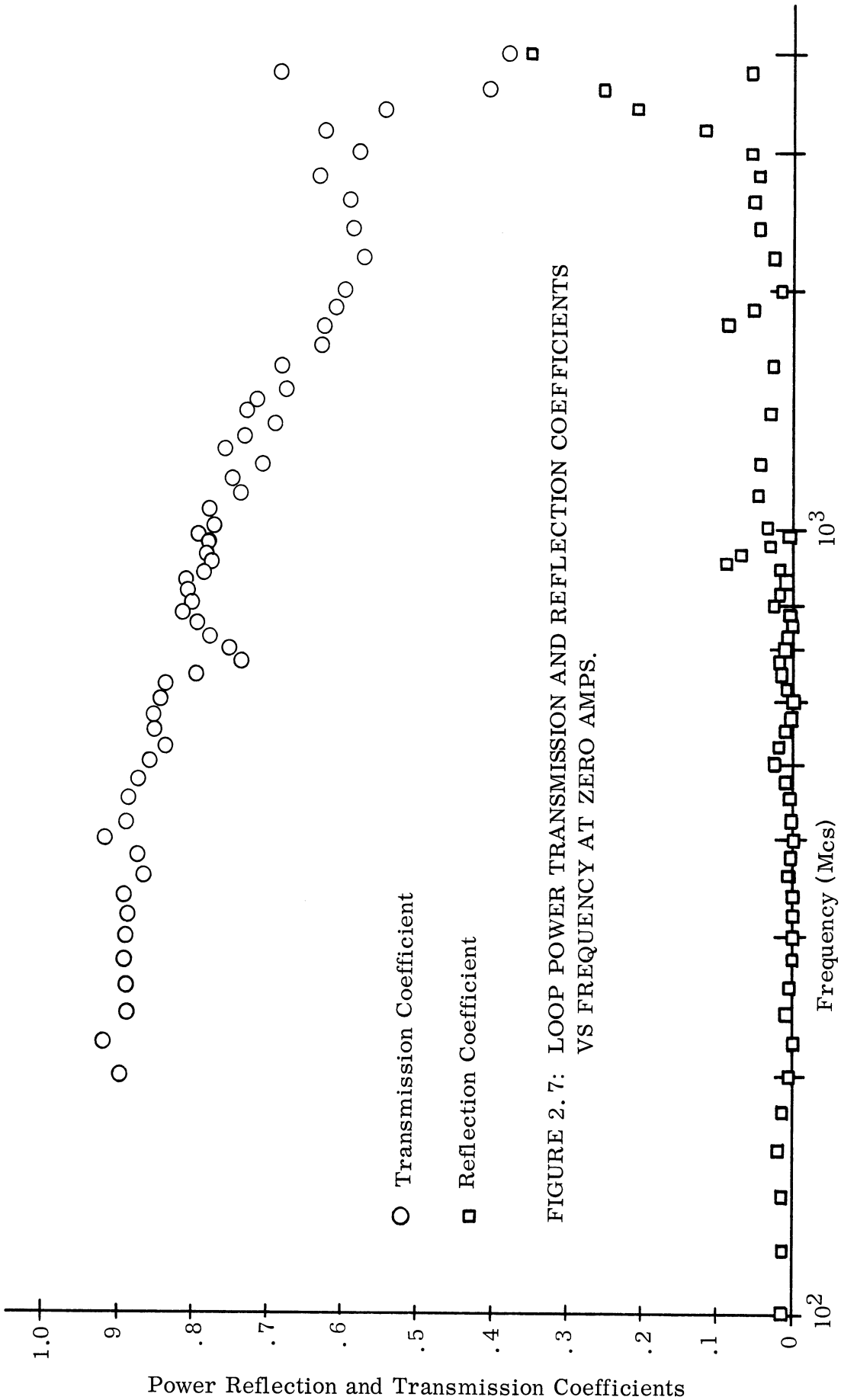

FIGURE 2.7: LOOP POWER TRANSMISSION AND REFLECTION COEFFICIENTS VS FREQUENCY AT ZERO AMPS.

The measurement of the power reflection coefficient of the diode is not as simple. The power reflection coefficient is first measured at the input terminal, and then transferred to the input of the coaxial diode. Obviously for this operation one must know the losses in the connecting line. The measured results of the attenuation (with the plate voltage off) between the input and the output terminals (i.e. for the entire circuit) are shown in Figure 2.8. The lower curve is computed from the skin depth loss formula by assuming reasonable wall conductivities and permeabilities. It exhibits the expected dependence on the square root of the frequency. A curve,which is a reasonable fit to the measured points shows the same frequency dependence, but the actual losses are about 1.5 times higher. This is not unusual in view of some uncertainty of the wall conductivity and especially of the permittivity of the nickel walls. The appropriate fraction of this loss was used to advance the refelection coefficient from the input terminal to the input of the diode.

The nominal length of the first cathode activated in the system was 14cm. The power reflection and transmission coefficients of this cathode as a function of frequency for anode currents of 0.5, 1.0 and 2.0 amperes (that were obtained at nominal anode voltages of 80, 120 and 190 volts respectively) are shown in Figures 2.9, 2.10 and 2.11. The nominal length of the second cathode was 20.3cm. The current densities were selected to correspond as closely as possible to the respective runs of the first cathode. This data is presented in Figures 2.9a, 2.10a and 2.11a.

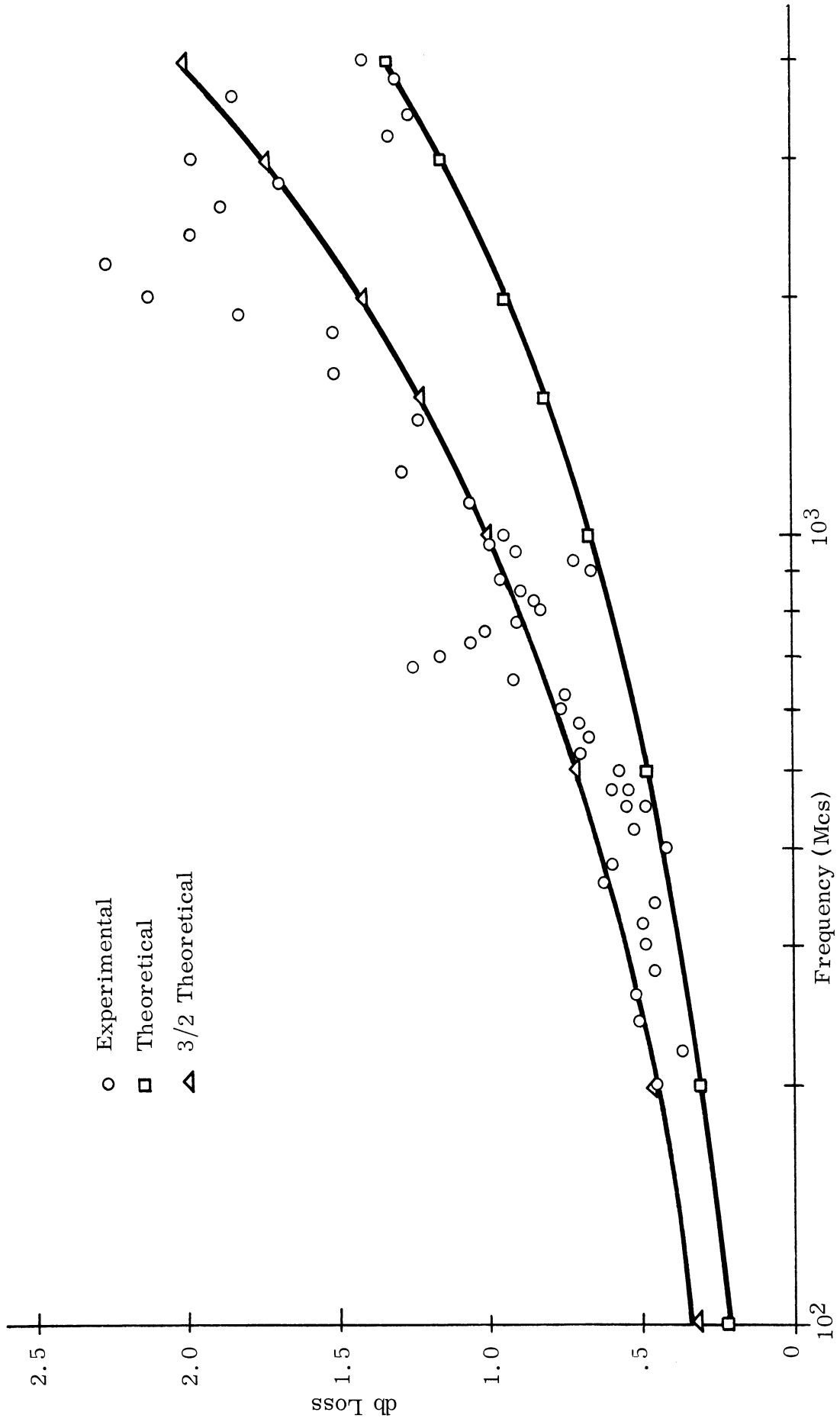

FIGURE 2.8: LOOP ATTENUATION LOSS VS FREQUENCY

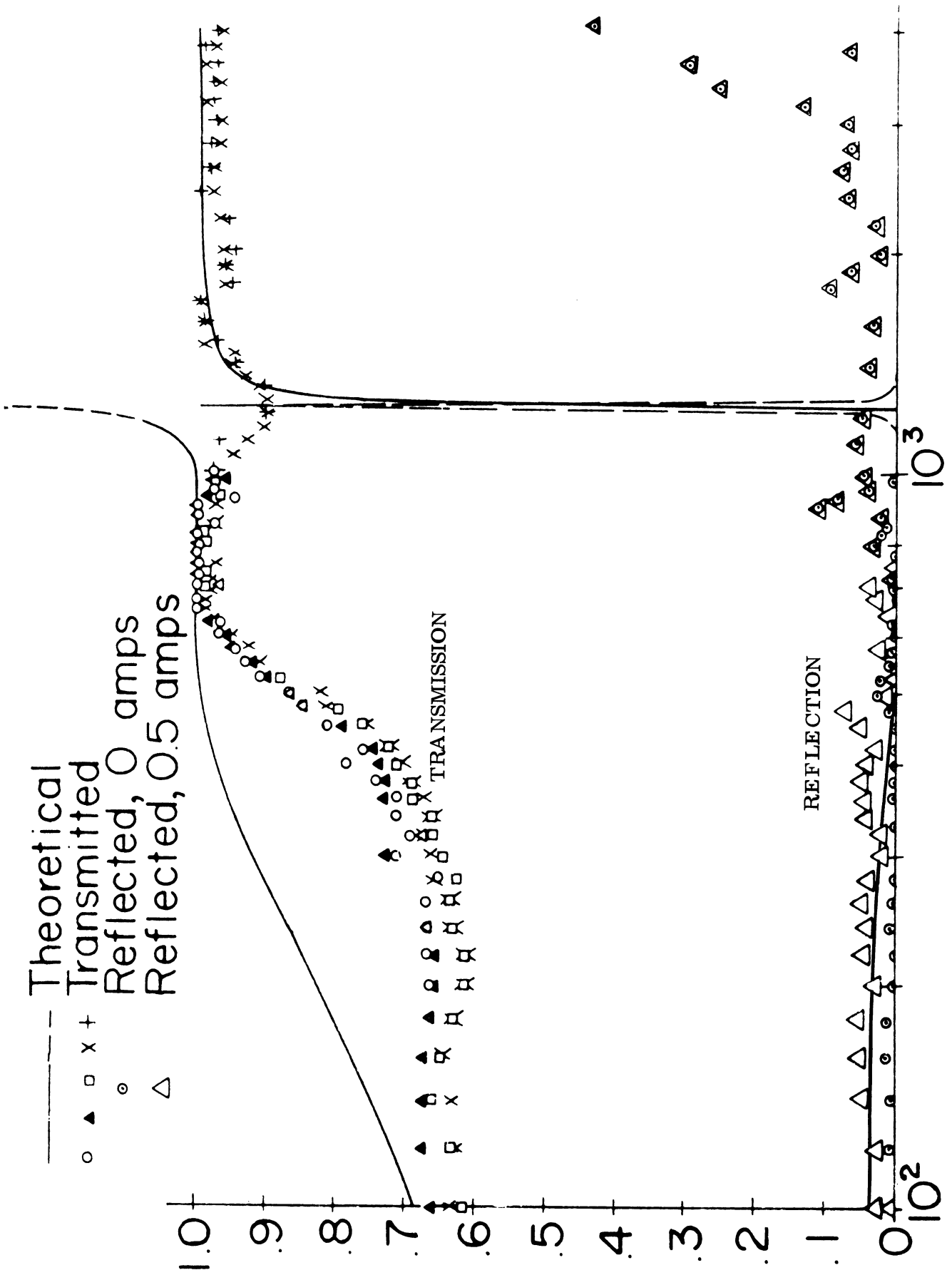

FIGURE 2.9: DIODE POWER REFLECTION AND TRANSMISSION COEFFICIENTS VS. FREQUENCY AT 0.5 AMP ANODE CURRENT (14 cm CATHODE)

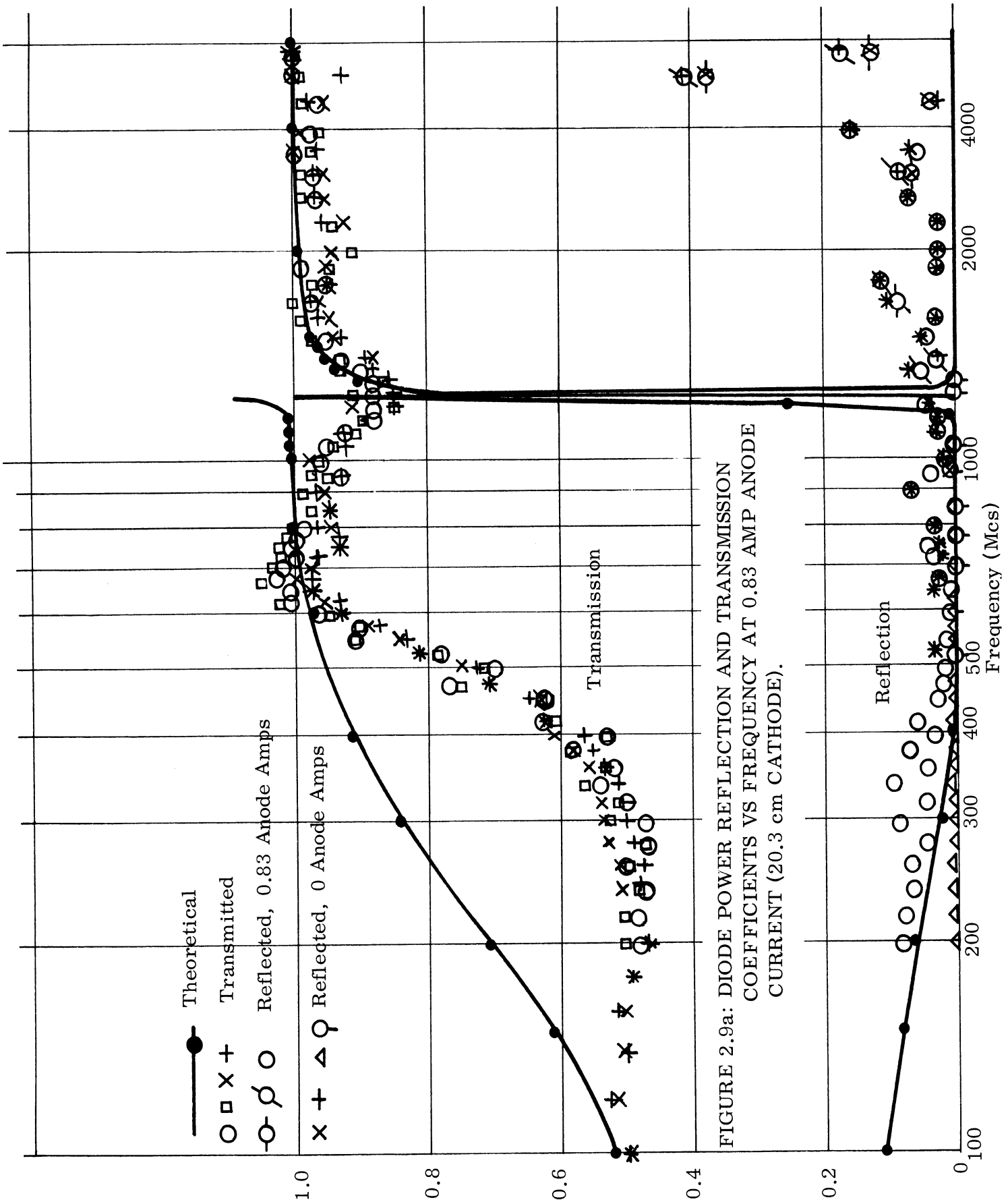

FIGURE 2.9a: DIODE POWER REFLECTION AND TRANSMISSION COEFFICIENTS VS FREQUENCY AT 0.83 AMP ANODE CURRENT (20.3 cm CATHODE).

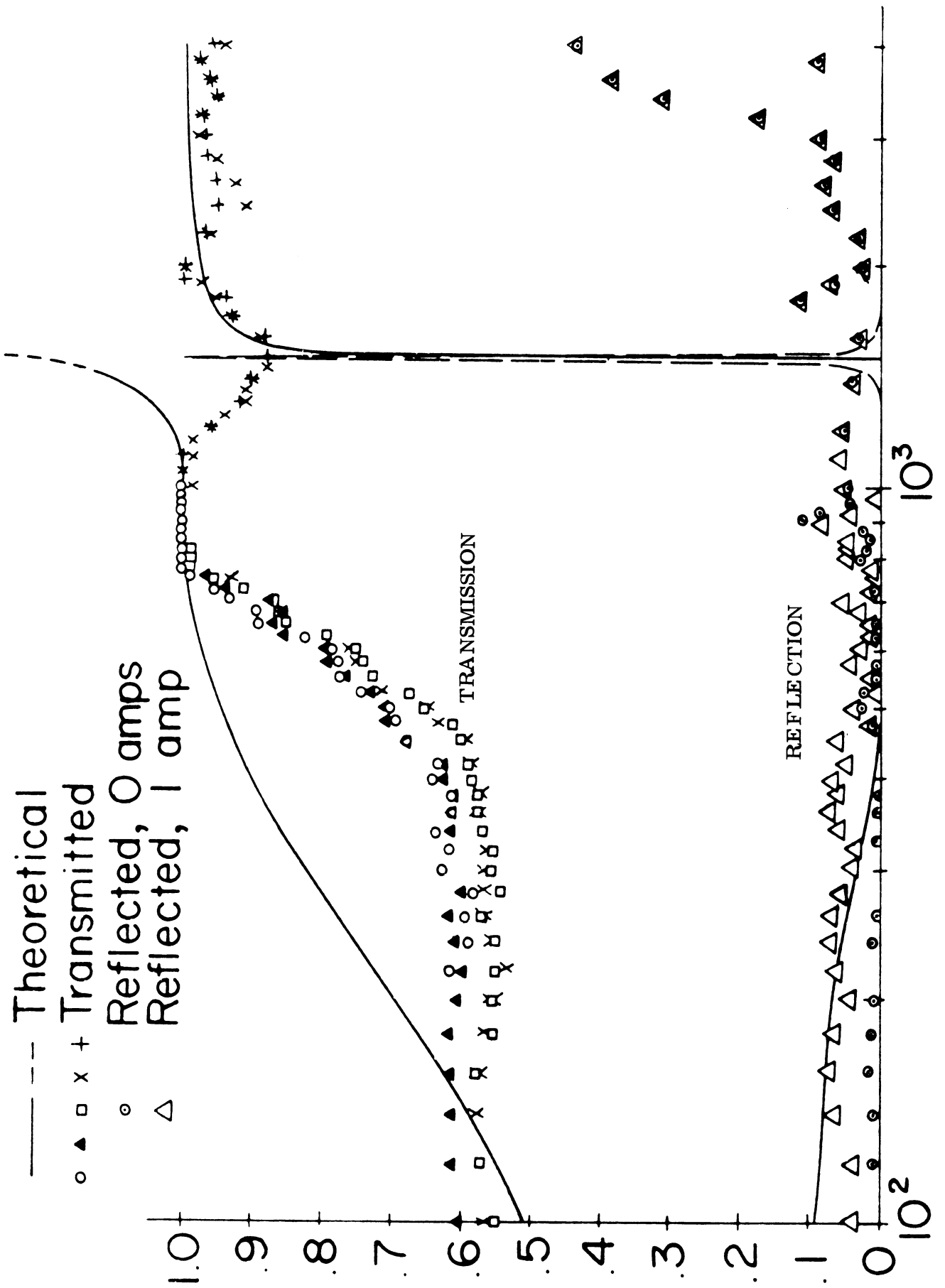

FIGURE 2.10: DIODE POWER REFLECTION AND TRANSMISSION COEFFICIENTS VS. FREQUENCY AT 1 AMP ANODE CURRENT (14 cm CATHODE)

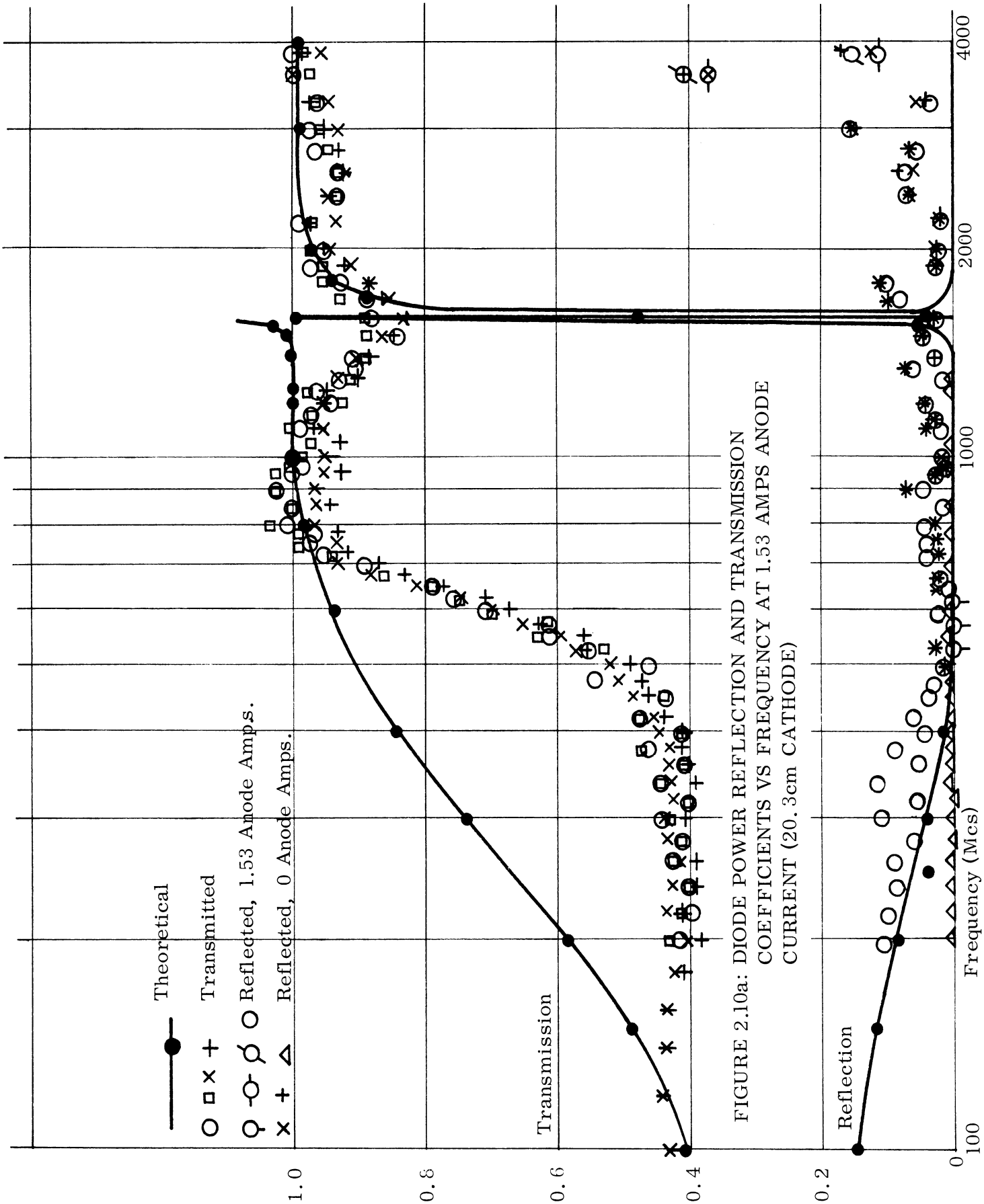

FIGURE 2.10a: DIODE POWER REFLECTION AND TRANSMISSION COEFFICIENTS VS FREQUENCY AT 1.53 AMPS ANODE CURRENT (20.3cm CATHODE)

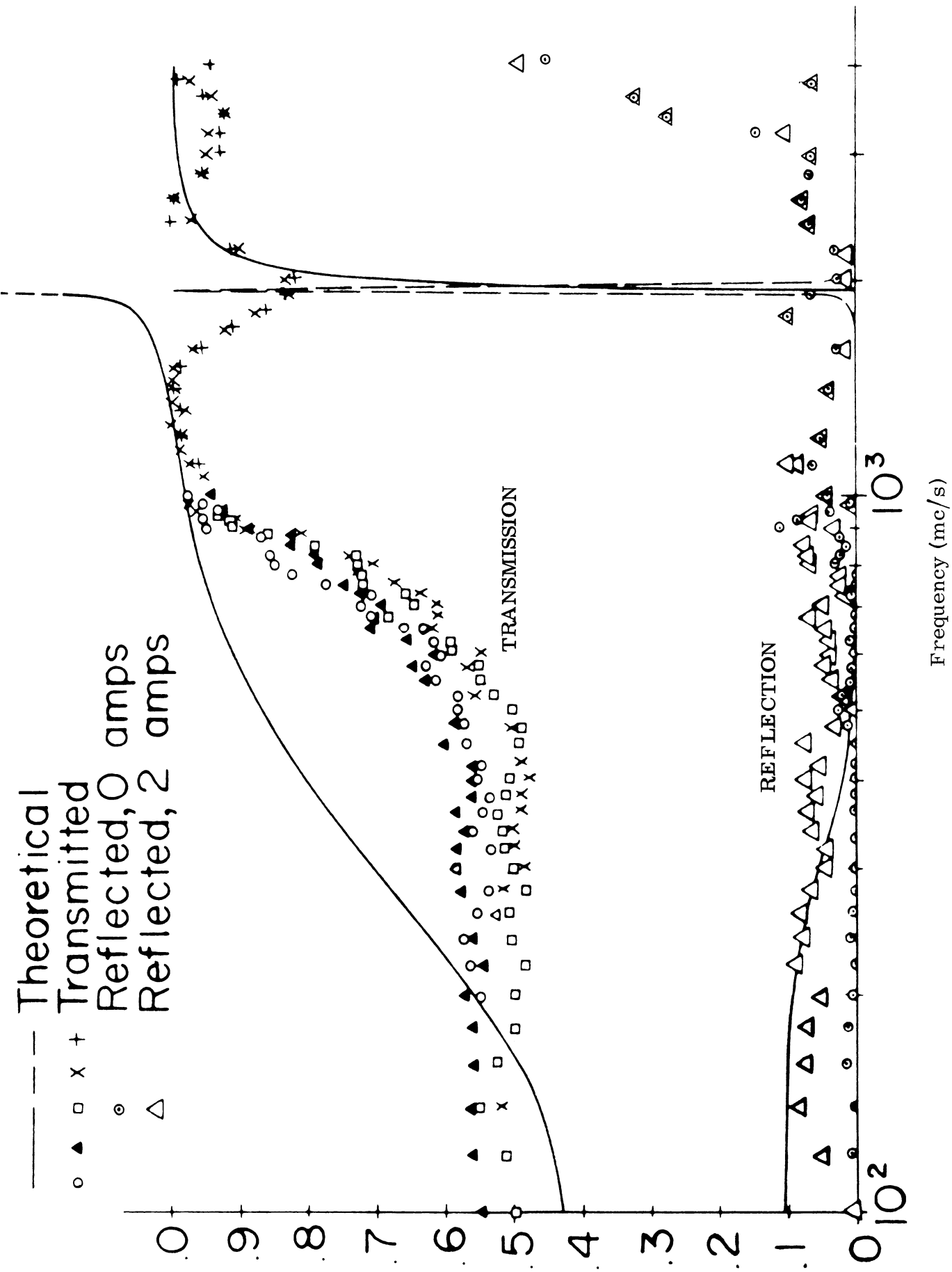

FIGURE 2.11: DIODE POWER REFLECTION AND TRANSMISSION COEFFICIENTS VS. FREQUENCY AT 2 AMPS ANODE CURRENT (14 cm CATHODE)

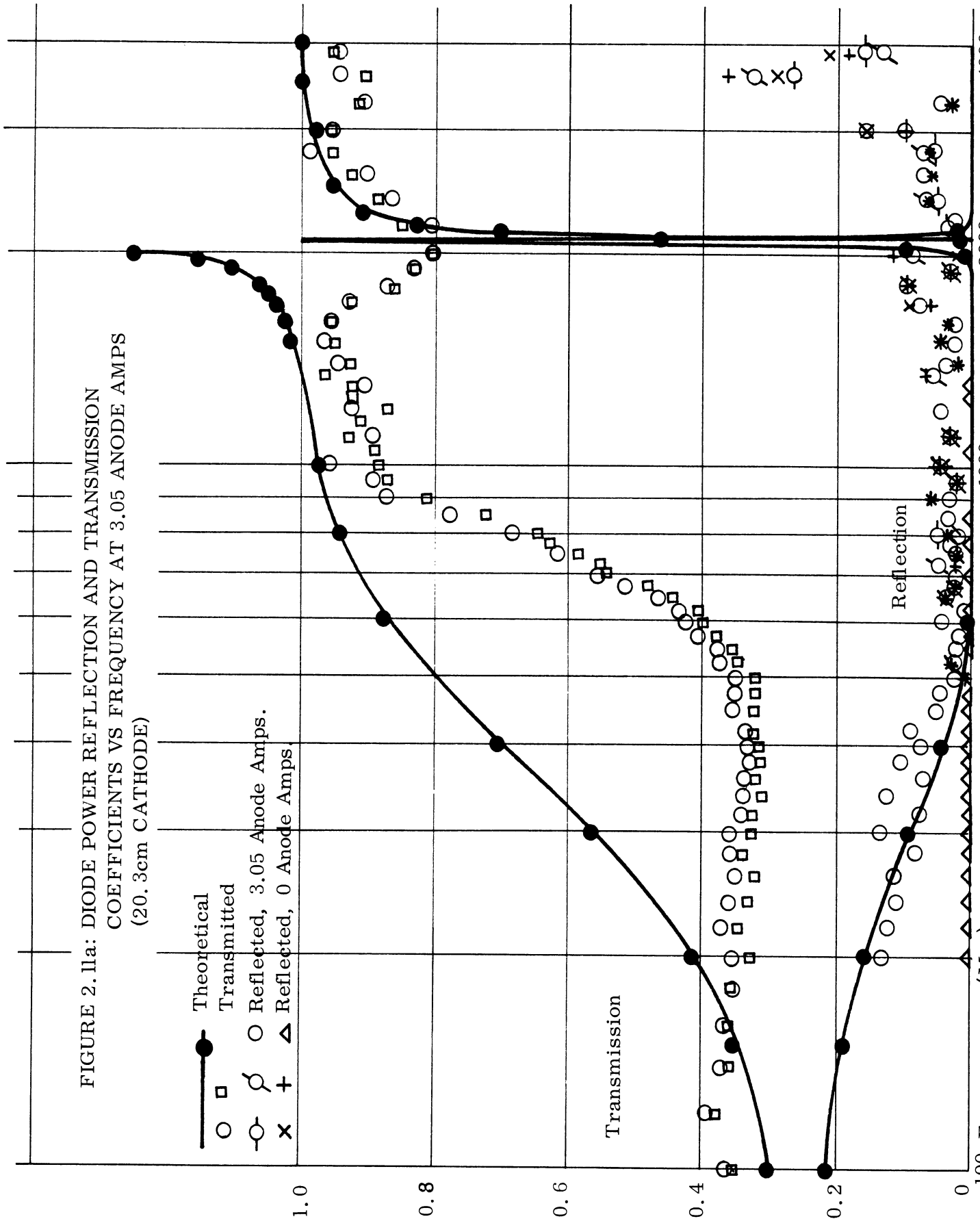

FIGURE 2.11a: DIODE POWER REFLECTION AND TRANSMISSION COEFFICIENTS VS FREQUENCY AT 3.05 ANODE AMPS (20.3cm CATHODE)

Note that good repeatability is obtained between the three or four runs shown. The accuracy of the measurements is of the order of $\pm$ 5 percent. The interesting features are, 1) the power transmission coefficient is flat over an appreciable frequency interval at lower frequencies, and 2) there is an absorption peak at a high frequency, and 3) the power reflection coefficient remains small at all times. For a lossless medium the power reflection transmission coefficients should add up to unity at all frequencies. Since this does not happen, it is clear that the electron stream appears as a lossy medium to the microwaves even up to fairly high frequencies.

In the coaxial configuration the interaction of the space charge limited electron stream with the incident electromagnetic field is a reasonably well defined boundary value problem. From the solution of Maxwell's equations subject to the appropriate boundary conditions one can predict the reflection and the transmission coefficients for the diode. However, the complete solution is of considerable difficulty and it still remains to be worked out. Only an approximate solution will be attempted here. The metal walls of the diode appear to the electrons as large molecules, and hence we may talk of electron-molecule collisions. The collisions between the electrons and the hypothetical molecules are inelastic whereby the total momentum of the electron is reduced to a low value. DC field intensity is sufficiently strong so that the drift velocity of the electrons

is large compared to the random velocity. The cathode to anode spacing constitutes the mean-free-path distance and the inverse of the DC electron transit time may be taken as the collision frequency (ν). The collision frequency absorption mechanism is normally derived for elastic collisions. Here we are arbitrarily extending the mechanism to a hypothetical gas with only inelastic collisions allowed.

As an example the plasma frequency in a 15 cm diode is given in Figure 2.12. These curves are computed from the electron densities obtained from the Child's law potential distribution in the diode. Using the hypothetical plasma picture we may say that the plasma frequency variation radially in the interelectrode space is a microscopic behavior, because it is on a scale smaller than the electron mean-free-path. In order to use the equivalent transmission line analysis we have to obtain a macroscopic parameter, i.e. an equivalent plasma frequency. If one approximates the plasma frequency in the diode by a step function, the lower value (f_2) given by the flat portion of the curves and the higher value (f_1), describing the conditions near the cathode, given by the location of the first absorption peak in the transmission curves, then one may obtain an equivalent plasma frequency from the solution of the principal mode (Klopfenstein, 1954). An alternate treatment is attempted in Appendix A of this report. Since the arguments of the characteristic equation for the principal mode in the region of interest are

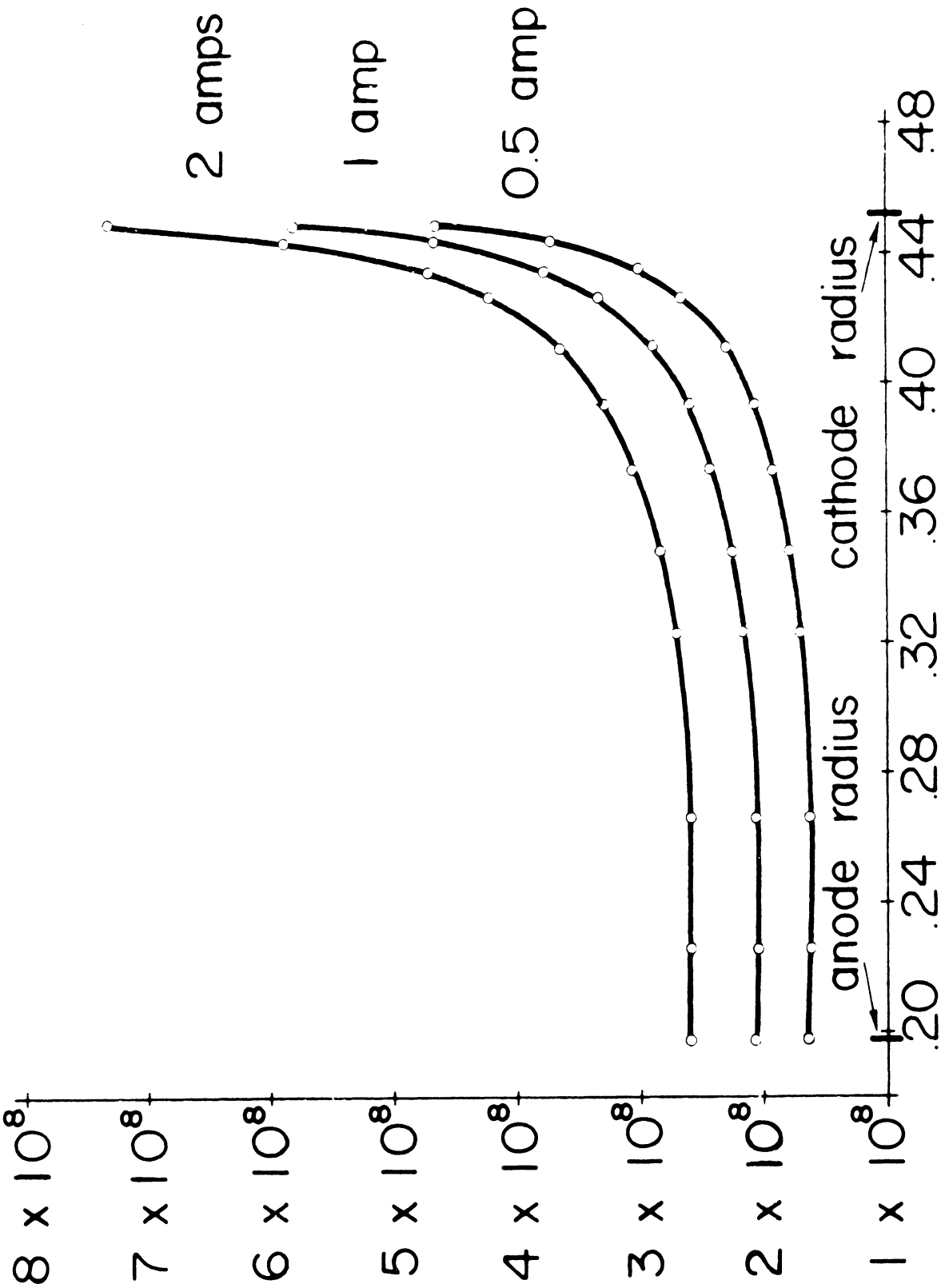

FIGURE 2.12: PLASMA FREQUENCY VS. DIODE RADIUS FOR DIFFERENT ANODE CURRENTS

considerably less than unity we may approximate both solutions of the Bessel's equation and of the modified Bessel's equations by the first terms in the series. This gives the plasma frequency in a very simple form:

$$(f_p/f)^2 = 1 - \frac{\left[1-(f_2/f)^2\right] \dfrac{\ln(r_c/r_a)}{\ln(r_o/r_a)}}{1+\dfrac{1-(f_2/f)^2}{1-(f_1/f)^2} \dfrac{\ln(r_c/r_o)}{\ln(r_o/r_a)}} \qquad (2\text{-}8)$$

where r_o denotes the position of the step in the electron density, and f is the frequency of the incident microwave radiation. The values of the parameters used in the subsequent calculations are summaried in Table 2.1.

TABLE 2.1 DIODE PARAMETERS

Figure	Anode Current(amps)	f_2 (cps)	f_1 (cps)	$\nu/2\pi$ (1/sec)
2.9	0.50	1.72×10^8	12.25×10^8	1.11×10^8
2.9a	0.83	1.79×10^8	12.25×10^8	1.11×10^8
2.10	1.00	2.09×10^8	15.0×10^8	1.35×10^8
2.10a	1.53	2.13×10^8	16.0×10^8	1.35×10^8
2.11	2.00	2.66×10^8	19.5×10^8	1.65×10^8
2.11a	3.05	2.70×10^8	21.0×10^8	1.65×10^8

$r_a = 0.198$cm, $r_o = 0.442$cm, $r_c = 0.452$cm

Having determined the effective plasma frequency f_p, and the collision frequency ν for the diode we may proceed to use the standard transmission line formulas presented in the previous section. The voltage transmission and

reflection coefficients, respectively, of such a medium of length, d, are given by equations (2-6a) and (2-6b). The squared amplitudes of (2-6a) and (2-6b) for the appropriate parameters given in Table 2.1, are shown either as solid or dashed curves in Figures 2.9 to 2.11a . The computed power transmission coefficient predicts absorption as the microwave frequency approaches the high plasma frequency close to the cathode. As f decreases sufficiently below f_1, then the right-hand side of (2-8) becomes negative (i.e. the effective plasma frequency for the diode is imaginary) and this together with the collision frequency predicts a growing wave. Therefore, the power transmission coefficient swings above unity. The power reflection coefficient in this area shows a spike approaching unity. As the microwave frequency approaches the lower plasma frequency, f_2, the power reflection coefficient increases and the power transmission coefficient decreases. However, the changes are not rapid enough to give a good fit to the measurements. For frequencies considerably above the lower plasma frequency the absorption is higher than predicted by the theory. For these frequencies the transmission and reflection behavior is only slightly influenced by the high plasma frequency near the cathode. The calculated power transmission curves level out only below 100 Mc.

The above model predicts the behavior at the high frequencies reasonably well, including the absorption. If a better approximation could be obtained which

incorporated the gradually changing character of the plasma frequency near the cathode, probably one could account fully for the absorption dip. The main difficulty is at the frequencies below f_1 . The predicted attenuation effects do not fall off fast enough to match the experimental curves. There does not appear to be any collision frequency which would predict this behavior.

Since the electron density variation in the inverted diode is relatively flat and since the first higher order mode occurs around 15 Gc, the solution of the transmission and reflection coefficients on the basis of the principal modes only is a reasonably good approximation. If the electron-wall interaction truly simulates inelastic gas collisions, then the data indicate that absorption from such collisions is greater than from the normal elastic collisions for a substantial frequency interval.

LIST OF SYMBOLS FOR SECTION III

$b_1 = \dfrac{2J\sqrt{p}}{\epsilon_o c_+}$

$b_2 = -\dfrac{2J\sqrt{p}}{\epsilon_o}\left(\dfrac{1}{c_+} + \dfrac{1}{c_-}\right)$

$b_3 = T_c - T_a$

$b_4 = T_a \log r_c - T_c \log r_a$

$c_{\pm} = \sqrt{\dfrac{e}{m_{\pm}}}\left(\dfrac{\varkappa_{\pm}}{2}\right)^{1/4}\sqrt{\dfrac{k}{\sigma_{\pm}\log\dfrac{r_c}{r_a}}}$

d = $r_c - r_a$ = cathode-anode spacing

e = magnitude of electronic charge

E = magnitude of the component of the electric field in the direction of the electron drift (radial direction in the present case)

I = total (net) current through the discharge

= current in external circuit

$\vec{j}_+$ = ion current density

$\vec{j}_-$ = electron current density

J = I/ℓ = current per unit length of cylinder

k = Boltzmann's constant

ℓ = length of cylinder

m_+ = ion mass

m_- = electron mass

n = number density of gas particles

p = gas pressure

r = radial coordinate (of cylindrical coordinates)

r_a = anode radius

r_c = cathode radius

T = gas temperature

T_a = anode temperature

T_c = cathode temperature

$\vec{v}_+$ = ion drift velocity

$\vec{v}_-$ = electron drift velocity

α_i = α = number of ionizing collisions suffered by one electron per unit path length in the field direction (first Townsend coefficient)

α_r = number of recombinations per second per unit volume per unit density of electrons per unit density of ions

ϵ_o = permittivity of free space

$\varkappa_+$ = fraction of the kinetic energy of an ion which it loses on the average in an elastic collision with a gas molecule

$\varkappa_-$ = fraction of the kinetic energy of an electron which it loses on the average in an elastic collision with a gas molecule

λ_+ = ion mean free path for elastic collisions

λ_- = electron mean free path for elastic collisions

$$\xi = \sqrt{\frac{T_c \log \frac{r}{r_a} - T_a \log \frac{r}{r_c}}{T_c - T_a}}$$

$$\xi_c = \sqrt{\frac{T_c \log \frac{r_c}{r_a}}{T_c - T_a}}$$

ρ_+ = positive charge density

ρ_- = magnitude of the negative charge density

σ_+ = total elastic collision cross section of the gas particles for ions

σ_- = total elastic collision cross section of the gas particles for electrons

Wherever the vector quantities $\vec{j}_{\pm}$ and $\vec{v}_{\pm}$ are written without the arrow, their absolute value is referred to.

In the first part of this Section, the case of no ionization is treated. Since no distinction between electrons and ions has to be made in that part, the quantities j_-, m_-, v_-, $\varkappa_-$, λ_-, ρ_-, σ_-, are used without the minus sign in the subscript. It is understood that these quantities refer to electrons.

III

THE ELECTRON DISTRIBUTION FUNCTION

3.1 Introduction

In order to deduce from experiment the correct relation between the electric properties of a plasma and its electron distribution, it is necessary to use an independent method for the determination of the distribution. The derivation of an expression for the electron density in terms of directly measurable observables is based on the fact that

$$\vec{j} = -\rho \vec{v} \ , \qquad (3\text{-}1)$$

where $\vec{j}$ = current density,

ρ = electron charge density,

$\vec{v}$ = electron drift velocity,

and the further fact that the drift velocity is determined by the gas temperature and pressure, the electric field, and the collision cross section of the gas molecules for electrons. The current density can easily be expressed in terms of the total current which is measurable. The electric field can be determined through Poisson's equation after the charge density has been eliminated from it, and the other quantities can all be measured directly so that the electron density can then be calculated. The minus sign in (3-1) is the result of the fact that $\vec{j}$ is in the direction of the conventional current, while $\vec{v}$ is in the direction of flow of the electrons. ρ is then defined as the absolute value of the electron charge density.

3.2 Case of No Ionization

To begin with the case of no ionization will be considered. Furthermore, it will be assumed that the only collisions which the electrons undergo are elastic. In that case the electron drift velocity is given by the expression

$$v = \sqrt{\frac{e}{m}} \left(\frac{\kappa}{2}\right)^{1/4} \sqrt{E\lambda}^{*} , \qquad (3\text{-}2)$$

where e = electronic charge,

m = electronic mass

κ = fraction of the kinetic energy of an electron which it loses on the average in an elastic collision with a gas molecule,

E = magnitude of the component of the electric field in the direction of the electron drift (radial direction in the present case),

λ = electron mean free path for elastic collisions.

The mean free path depends on the total elastic collision cross section σ of the molecules for the electrons in the following way

$$\lambda = \frac{1}{n\sigma} , \qquad (3\text{-}3)$$

where n is the number density of gas molecules. But the equation of state is

$$n = \frac{p}{kT} , \qquad (3\text{-}4)$$

where T is the absolute temperature of the gas and k is Boltzmann's constant. Substituting equations (3-3) and (3-4) into (3-2) one obtains the expression

* See for example equation (4.21) in von Engel (1955).

$$v = \sqrt{\frac{e}{m}} \left(\frac{\varkappa}{2} \right)^{1/4} \sqrt{\frac{kT}{\sigma}} \sqrt{\frac{E}{p}} \quad . \tag{3-5}$$

In the present investigation the temperature is a function of position, since a hot cathode discharge is being used. Let the cathode radius and temperature be r_c and T_c respectively and the corresponding values for the anode r_a and T_a. If the outer cylinder is the cathode, then $r_c > r_a$. In the steady state the temperature distribution inside the gas is given by the time-independent Fourier law, which is in cylindrical coordinates

$$\nabla^2 T = \frac{1}{r} \frac{d}{dr} \left(r \frac{dT}{dr} \right) = 0 \, , \tag{3-6}$$

where the heating of the gas due to electron-molecule collisions has been neglected and the temperature has been considered a function of r only. This latter assumption implies that the cylinder is taken to be of infinite length since the variation of T with respect to z near the bases of the cylinder has been neglected. The gas temperatures at the radii r_c and r_a are T_c and T_a respectively. Solution of equation (3-6) for those boundary conditions gives the following temperature distribution:

$$T = \frac{1}{\log \frac{r_c}{r_a}} \left(T_c \log \frac{r}{r_a} - T_a \log \frac{r}{r_c} \right) \, , \tag{3-7}$$

where

$$r_c \gtrsim r \gtrsim r_a \quad .$$

If this expression for the temperature is substituted into (3-5), the drift velocity

becomes

$$v = c\sqrt{T_c \log \frac{r}{r_a} - T_a \log \frac{r}{r_c}}\ \sqrt{\frac{E}{p}}\ , \tag{3-8}$$

where

$$c = \sqrt{\frac{e}{m}}\ \left(\frac{\varkappa}{2}\right)^{1/4} \sqrt{\frac{k}{\sigma \log \frac{r_c}{r_a}}} \tag{3-9}$$

is a constant.

Noting that the current density and radius vectors are parallel we have

$$I = 2\pi \ell\, \vec{r} \cdot \vec{j} = 2\pi \ell\, r\, j$$

$$j = \frac{I}{2\pi r \ell} = \frac{J}{2\pi r}\ , \tag{3-10}$$

where

I = current in external circuit

J = I/ℓ = current per unit length of cylinder,

ℓ = length of cylinder,

and j and r are the magnitudes of $\vec{j}$ and $\vec{r}$ respectively. Scalar multiplication of (3-1) by $2\pi \vec{r}$ yields

$$2\pi r j = J = 2\pi\, r\, \rho\, v\ , \tag{3-11}$$

where the minus sign on the right hand side disappears because the vectors $\vec{r}$ and $\vec{v}$ have opposite directions. Substituting (3-8) into (3-11) one obtains

$$\rho = \frac{J}{2\pi r c \sqrt{T_c \log \frac{r}{r_a} - T_a \log \frac{r}{r_c}}\ \sqrt{\frac{E}{p}}}\ . \tag{3-12}$$

Hence Poisson's equation becomes in terms of the electric field

$$\frac{1}{r}\frac{d}{dr}(r\,E) = -\frac{4\pi}{\epsilon_o}\rho$$

$$\frac{1}{r}\frac{d}{dr}(r\,E) = -\frac{2\,J}{r\,\epsilon_o\,c\sqrt{T_c \log\frac{r}{r_a} - T_a \log\frac{r}{r_c}}\ \sqrt{\frac{E}{p}}}\ ,$$

where ϵ_o is the permittivity of free space and the minus sign results from the fact that ρ is the absolute value of a negative charge density. Carrying out the differentiation and regrouping terms yields

$$E^{3/2} + r\sqrt{E}\,\frac{dE}{dr} = -\frac{2\,J\sqrt{p}}{\epsilon_o c\sqrt{T_c \log\frac{r}{r_a} - T_a \log\frac{r}{r_c}}}$$

Now let

$$E^{3/2} = Y,$$
$$\log r = z,$$
$$\log r_a = z_a,$$
$$\log r_c = z_c\ .$$

Then the above differential equation becomes

$$\frac{dY}{dz} + \frac{3}{2}Y + \frac{3\,J\sqrt{p}}{\epsilon_o\,c\sqrt{T_c(z-z_a) - T_a(z-z_c)}} = 0$$

with the boundary condition

$$Y = 0 \text{ at } z = z_c\ .$$

The solution of this equation is

$$Y = -\frac{3J\sqrt{p}}{\epsilon_o c} e^{-\frac{3}{2}z} \int_{z_c}^{z} \frac{e^{\frac{3}{2}t}}{\sqrt{T_c(t - z_a) - T_a(t - z_c)}} dt \quad * .$$

Now let

$$\frac{T_c(t - z_a) - T_a(t - z_c)}{T_c - T_a} = x_1^2 .$$

Then

$$dt = 2 x_1 dx_1 ,$$

and Y becomes

$$Y = \frac{6J\sqrt{p}}{\epsilon_o c\sqrt{T_c - T_a}} e^{\frac{3}{2}\frac{T_c(z_a - z) - T_a(z_c - z)}{T_c - T_a}} \int_{x}^{x_c} e^{\frac{3}{2}x_1^2} dx_1 ,$$

where

$$x = \sqrt{\frac{T_c(z - z_a) - T_a(z - z_c)}{T_c - T_a}} ,$$

$$x_c = \sqrt{\frac{T_c(z_c - z_a)}{T_c - T_a}}$$

* See for example Kamke (1959), page 16.

and the minus sign on the right hand side has been absorbed by interchanging the limits of integration. Hence, the electric field as a function of radius is

$$E = \left\{ \frac{6\,J\,\sqrt{p}}{\epsilon_o\, c\,\sqrt{T_c - T_a}} \frac{(r_a)^{\frac{3}{2}} \frac{T_c}{T_c - T_a}}{(r_c)^{\frac{3}{2}} \frac{T_a}{T_c - T_a}} r^{-\frac{3}{2}} \int_{\xi}^{\xi_c} e^{\frac{3}{2}x_1^2}\, dx_1 \right\}^{\frac{2}{3}}, \quad (3\text{-}13)$$

where

$$\xi = \sqrt{\frac{T_c \log \frac{r}{r_a} - T_a \log \frac{r}{r_c}}{T_c - T_a}},$$

$$\xi_c = \sqrt{\frac{T_c \log \frac{r_c}{r_a}}{T_c - T_a}}.$$

Since the integral appearing in (3-13) cannot be evaluated in closed form, either a numerical integration has to be performed, or the integrand has to be approximated. Two methods of approximation, one for large x_1 and one for small x_1 will be briefly discussed in the appendix to this section.

We are now in a position to write down the expression for the charge density. Substituting equation (3-13) into equation (3-12) and simplifying the resulting expression, one finally obtains

$$\rho = \frac{1}{2\pi}\left[\frac{\epsilon_o I^2 p \sqrt{T_c - T_a}}{6 \ell^2 c^2}\right]^{1/3} \frac{(r_c)^{\frac{1}{2}\frac{T_a}{T_c - T_a}} (r_a)^{-\frac{1}{2}\frac{T_c}{T_c - T_a}}}{\sqrt{r\left[T_c \log\frac{r}{r_a} - T_a \log\frac{r}{r_c}\right]}} \left\{\int_{\xi}^{\xi_c} e^{\frac{3}{2}x_1^2} dx_1\right\}^{-\frac{1}{3}} . \tag{3-14}$$

Equation (3-14) expresses the charge density in terms of either directly measurable observables or fundamental constants except for the two quantities $\varkappa$ and σ , which have to be obtained phenomenologically from published data. $\varkappa$ for several gases may for example be obtained from Fig. 63 of vonEngel (1955), where the constant values of $\varkappa$ for low $\frac{E}{p}$ are applicable here since they refer to the case of no inelastic collisions, which has also been assumed in the present investigation.

3.3 Introduction of Ionization

In order to take the effect of ionization into account, the positive and negative charge densities ρ_+ and ρ_- are introduced. The corresponding current densities are j_+ and j_-. The positive (negative) sign in the subscripts here and in other quantities implies that said quantities refer to ions (electrons). Although the gas as a whole may be neutral, this is not true of the local charge density because of the d.c. field. The electric field, charge, and current densities are related by the following equations

$$\frac{1}{r}\frac{d}{dr}(rE) = \frac{4\pi}{\epsilon_o}(\rho_+ - \rho_-), \tag{3-15}$$

$$r\frac{dj_-}{dr} + j_- + r\left(\alpha_i j_- - \frac{\alpha_r}{e}\rho_+\rho_-\right) = 0, \tag{3-16}$$

$$r\frac{dj_+}{dr} + j_+ - r\left(\alpha_i j_- - \frac{\alpha_r}{e}\rho_+\rho_-\right) = 0, \tag{3-17}$$

where $j_{\pm} = \rho_{\pm} v_{\pm}$ = magnitudes of ion (electron) current densities,

α_i = number of ionizing collisions suffered by one electron per unit path length in the field directions (first Townsend coefficient),

α_r = number of recombinations per second per unit volume per unit density of electrons per unit density of ions,

and $v_{\pm}$ are the drift velocities of the ions and electrons.

Equations (3-16) and (3-17) express the conservation of electrons and ions respectively. The ionization coefficient α_i depends on the ionization cross section and the gas density. Because of the dependence of the ionization cross section on electron energy, α_i is also a function of electron energy and thus of $\frac{E}{p}$. It will be assumed that recombination is negligible compared with ionization. This is reasonable, since ionization is caused by electron-neutral collisions, while recombination is generally caused by three-body electron-neutral-ion collisions, and the degree of ionization is considered low in the present treatment. Hence, equations (3-16) and

(3-17) simplify to

$$r \frac{dj_-}{dr} + j_- + \alpha r j_- = 0, \tag{3-16a}$$

$$r \frac{dj_+}{dr} + j_+ - \alpha r j_- = 0, \tag{3-17a}$$

where now the subscript i on α has been dropped.

The physical picture described by equations (3-16a) and (3-17a) is that of a stream of electrons traveling from cathode to anode and causing an avalanche due to ionization. The current at the anode is entirely an electron current. The current at the cathode has both an ion and an electron component. The number of electrons emitted by the cathode per second plus the number of ions hitting the cathode per second and becoming neutralized equals the number of electrons which are incident at the anode per second. Hence, the difference between the electron currents at the anode and at the cathode equals the ion current at the cathode, which in turn equals the number of ionizations per second in the entire gas, since ions do not accumulate and diffusion to the cathode is assumed to be the only mechanism for the removal of ions.

The solutions of equations (3-16a) and (3-17a) for the boundary conditions

$$2 \pi r_a \ell j_- (r_a) = I$$

and

$$j_+ (r_a) = 0$$

are

$$j_-(r) = \frac{I}{2\pi r \ell} e^{-\alpha(r-r_a)}, \tag{3-18}$$

$$j_+(r) = \frac{I}{2\pi r \ell} \left[1 - e^{-\alpha(r-r_a)}\right], \tag{3-19}$$

where I is again the current in the external circuit.

In the integrations of equations (3-16a) and (3-17a) α has been considered constant. This is not strictly true since the electric field and therefore also the electron energy are functions of position and α is a function of electron energy. For the elementary treatment presented here a suitably chosen average value of α should however be satisfactory. Equation (3-18) describes an electron avalanche. To see this, one merely has to write down the ratio of the electron current at the anode to that at the cathode, which is

$$\frac{I_-(r_a)}{I_-(r_c)} = \frac{2\pi r_a \ell j_-(r_a)}{2\pi r_c \ell j_-(r_c)} = e^{-\alpha(r_a-r_c)} .$$

Hence,

$$I_-(r_a) = I_-(r_c)\, e^{\alpha d} ,$$

where d is the radial distance from the cathode to anode.

It will now be assumed that the electron drift velocity is determined solely by the electric field and the elastic electron-neutral collisions. This is reasonable since the average electron energy is considerably below the ionization and even

excitation, potentials. Therefore only the very small fraction of electrons in the high energy tail of the distribution will undergo inelastic collisions, and the overwhelming majority of electrons will suffer elastic collisions only . The same is of course true of the ions. The drift velocities of ions and electrons are therefore given by equation (3-5), viz

$$v_+ = \sqrt{\frac{e}{m_+}}\left(\frac{\varkappa_+}{2}\right)^{1/4}\sqrt{\frac{kT}{\sigma_+}}\sqrt{\frac{E}{p}}\,, \tag{3-20}$$

$$v_- = \sqrt{\frac{e}{m_-}}\left(\frac{\varkappa_-}{2}\right)^{1/4}\sqrt{\frac{kT}{\sigma_-}}\sqrt{\frac{E}{p}}\,, \tag{3-21}$$

where m_+ is the mass of the ions and $\varkappa$ and λ have been defined following equation (3-2). Substituting the above relations for the drift velocities into the expressions for the current densities, one obtains

$$j_\pm = \rho_\pm \sqrt{\frac{e}{m_\pm}}\left(\frac{\varkappa_\pm}{2}\right)^{1/4}\sqrt{\frac{kT}{\sigma_\pm}}\sqrt{\frac{E}{p}} = \rho_\pm c_\pm \sqrt{T_c \log\frac{r}{r_a} - T_a \log\frac{r}{r_c}}\sqrt{\frac{E}{p}}\,, \tag{3-22}$$

where (3-3), (3-4) and (3-7) have been used and

$$c_\pm = \sqrt{\frac{e}{m_\pm}}\left(\frac{\varkappa_\pm}{2}\right)^{1/4}\sqrt{\frac{k}{\sigma_\pm \log\frac{r_c}{r_a}}}\,. \tag{3-23}$$

$\sigma_\pm$ are the total elastic collision cross sections of the neutral particles for ions and electrons respectively. The positive and negative charge densities follow from equations (3-18), (3-19) and (3-22) and are given by the expressions

$$\rho_+ = \frac{J\left[1-e^{-\alpha(r-r_a)}\right]}{2\pi r c_+\sqrt{T_c\log\frac{r}{r_a}-T_a\log\frac{r}{r_c}}\sqrt{\frac{E}{p}}} \quad , \tag{3-24}$$

$$\rho_- = \frac{J\, e^{-\alpha(r-r_a)}}{2\pi r c_-\sqrt{T_c\log\frac{r}{r_a}-T_a\log\frac{r}{r_c}}\sqrt{\frac{E}{p}}} \quad , \tag{3-25}$$

where again $J = I/\ell$.

Substitution of (3-24) and (3-25) into (3-15) yields finally

$$\sqrt{E}\,\frac{d}{dr}(rE) = \frac{2J\sqrt{p}}{\epsilon_o\sqrt{T_c\log\frac{r}{r_a}-T_a\log\frac{r}{r_c}}}\left[\frac{1}{c_+}(1-e^{-\alpha(r-r_a)})-\frac{1}{c_-}e^{-\alpha(r-r_a)}\right] \quad . \tag{3-26}$$

Again introducing the transformation

$$E^{3/2} = Y$$

one obtains a differential equation of the form

$$\frac{dY}{dr}+\frac{3}{2}\frac{1}{r}Y = \frac{3}{2}\,\frac{b_1+b_2\,e^{-\alpha(r-r_a)}}{r\sqrt{b_3\log r+b_4}} \quad , \tag{3-27}$$

where

$$b_1 = \frac{2J\sqrt{p}}{\epsilon_o c_+} \quad ,$$

$$b_2 = -\frac{2J\sqrt{p}}{\epsilon_o}\left(\frac{1}{c_+}+\frac{1}{c_-}\right) \quad ,$$

$$b_3 = T_c-T_a \quad ,$$

$$b_4 = T_a\log r_c-T_c\log r_a \quad .$$

The general solution of (3-27) for the boundary condition $Y(r_c)=0$ is

$$Y = E^{3/2} = \frac{1}{r^{3/2}} \int_{r_c}^{r} \frac{b_1 + b_2 e^{-\alpha(\rho - r_a)}}{\sqrt{b_3 \log \rho + b_4}} \sqrt{\rho}\, d\rho \quad . \tag{3-28}$$

A remark concerning the sign of Y is in order at this point. Since ρ_+ and ρ_- are the absolute values of the charge densities, it is clear that the positive square root of E enters into equations (3-24) and (3-25). But a cursory inspection of the integral appearing in (3-28) will reveal that it may be either positive or negative depending on the upper limit r, and if the integral is negative, then $\sqrt{E} < 0$. In order to insure that one obtains the positive square root of E, one has to take the absolute value of the integral when the expression for $\sqrt{E}$ is substituted into the expressions for ρ_+ and ρ_- .

The integral in (3-28) can be written as the sum of two integrals. The first of these can again be reduced to an integral of the type $\int e^{x^2} dx$ by the substitutions $\log \rho = z$ and $\frac{b_3 z + b_4}{b_3} = x^2$. The second integral can frequently also be reduced to such an integral if a power series expansion of the exponential function is practical. To show this, consider the integral

$$j = \int \rho^n \frac{\sqrt{\rho}}{\sqrt{b_3 \log \rho + b_4}}\, d\rho \quad ,$$

where ρ^n (n integer) is proportional to a typical term in the expansion of $e^{-\alpha(\rho - r_a)}$. Let $\log \rho = z$.

Then

$$j = \int \frac{e^{\frac{2n+3}{2} z}}{\sqrt{b_3 z + b_4}} \, dz \quad .$$

Again let

$$\frac{b_3 z + b_4}{b_3} = x^2 \quad .$$

Then

$$j = 2 \int e^{\frac{2n+3}{2}(x^2 - b_4/b_3)} \, dx = 2 e^{-\frac{2n+3}{2} \frac{b_4}{b_3}} \int e^{\frac{2n+3}{2} x^2} \, dx \quad .$$

In many practical applications only a few terms of the exponential series are required to achieve convergence. For example in our investigation E/p is of the order of 200 volts/(cm x mm Hg). From Figures 4.34a and 4.35 of Brown (1959) it follows that the corresponding value of α/p for both helium and nitrogen is of the order of 1(cm x mm Hg)$^{-1}$. Since a pressure of 1mm Hg has been used, $\alpha \cong 1$ cm^{-1} in both cases. Since, furthermore $\rho - r_a$ varies from 0 to 0.245cm, the exponent $\alpha(\rho - r_a)$ is obviously sufficiently small for convergence to occur after only a few terms depending on the accuracy desired.

The electron charge density is again obtained by substituting the expression for E from (3-28) into (3-25) . After simplifying this yields

$$\rho_- = \frac{1}{2\pi} \left[\frac{\epsilon_o I^2 p c_+}{3 \ell^2 c_-^2}\right]^{1/3} \frac{e^{-\alpha(r - r_a)}}{\sqrt{r(T_c \log \frac{r}{r_a} - T_a \log \frac{r}{r_c})}} \left\{ \int_{r_c}^{r} \frac{c_- - (c_+ + c_-) e^{-\alpha(\rho - r_a)}}{\sqrt{T_c \log \frac{\rho}{r_a} - T_a \log \frac{\rho}{r_c}}} \sqrt{\rho} \, d\rho \right\}^{-\frac{1}{3}} \quad . \tag{3-29}$$

Similarly the positive charge density is

$$\rho_+ = \frac{1}{2\pi}\left[\frac{\epsilon_o I^2 p c_-}{3 \ell^2 c_+^2}\right]^{1/3} \frac{1 - e^{-\alpha(r-r_a)}}{\sqrt{r(T_c \log\frac{r}{r_a} - T_a \log\frac{r}{r_c})}} \left\{\left| \int_{r_c}^{r} \frac{c_- - (c_+ + c_-)e^{-\alpha(\rho - r_a)}}{\sqrt{T_c \log\frac{\rho}{r_a} - T_a \log\frac{\rho}{r_c}}} \sqrt{\rho}\, d\rho \right|\right\}^{-\frac{1}{3}} . \tag{3-30}$$

It is easy to check that, if α=0 (no ionization), then ρ_+=0 and ρ_- goes over into the relation (3-14) after the appropriate change in the variable of integration.

The basic physical assumptions made in the derivation of the above expressions for the charge densities are summarized below.

1) Electron-ion recominations are negligible

2) The ionization coefficient α used in this treatment is a suitably chosen mean value.

3) The electron drift velocity is determined only by the balance between the elastic electron-neutral collisions and the acceleration of the electrons by the electric field. Since the drift velocity is the average of the electron velocity components in the direction of the electric field, this assumption means that in computing this average the distribution is cut off at the minimum energy necessary to cause excitation. The assumption is therefore valid only if the mean energy of the electrons is considerably below the lowest excitation potential of the atoms (or molecules) in question since in that case only the high energy tail of the distribution function would be neglected.

4) The fractional change in electric field over one mean free path is small, i.e.

$$\left|\frac{\lambda}{E}\frac{dE}{dr}\right| << 1.$$

This is implied in the derivation of the expression (3-2) for the drift velocity.

5) The fractional energy loss per collision $\varkappa$ is not a function of the electric field. As long as elastic collisions only are considered, this assumption is correct as can be seen from Figure 63 of von Engel (1955). In the case of inelastic collisions this assumption no longer holds true. But since according to assumption 3) the expression for the drift velocity used here is based on the absence of inelastic collisions, this last assumption is therefore consistent with the rest of the treatment.

In conclusion a short discussion of the expressions for the positive and negative charge densities together with a few suggestions for further work will be given.

First of all it is immediately obvious that both the expression for ρ_+ and that for ρ_- diverge as $r \to r_c$. This is a consequence of the relations for the drift velocities (3-20) and (3-21). According to these, $v_{\pm} = 0$ if $E = 0$, and the electric field has been taken as zero at the cathode. Since neither of the current densities vanishes at the cathode, the charge densities obviously become infinite, if the drift velocities vanish. The electrons naturally do not leave the cathode with zero velocity but rather with a Maxwellian velocity distribution which is determined by the cathode temperature. Furthermore the assumption of a slowly varying electric field is especially bad in the region near the cathode. In particular the electric field does not vanish at the cathode but, because of the space charge, a certain distance away from the cathode. The region where the electric field

vanishes is referred to as the virtual cathode. Because of the divergence of the expressions for the charge densities at the cathode, these expressions hold throughout the discharge (provided the stated assumptions are satisfied) but excluding the small region immediately adjacent to the cathode. Additional work is required to generalize the expression for the current density by removing the above mentioned objections. A correct treatment would of course result in a finite value for the charge densities at the cathode.

According to the fourth assumption above the fractional change in electric field over one mean free path must be small. Because of the cylindrical geometry considered in the present treatment E is obviously never constant. In a vacuum and in the absence of any discharge (i.e. no space charge) the electric field is proportional to $1/r$ and therefore

$$\left|\frac{\lambda}{E}\frac{dE}{dr}\right| = \frac{\lambda}{r} \quad .$$

The necessary and sufficient condition for the fourth assumption to be satisfied is therefore

$$\lambda \ll r_a \quad .$$

The total charge in the gas is given by

$$Q = \int_V (\rho_+ - \rho_-) dV, \tag{3-31}$$

where the integration has to be carried out over the volume occupied by the discharge. From (3-29) and (3-30) one sees that the integrand $(\rho_+ - \rho_-)$ equals a

positive definite factor multiplied by the expression

$$\Delta \equiv -(c_+ + c_-)e^{-\alpha(r-r_a)} + c_- \quad .$$

Δ is negative in the region

$$r_a \leqq r < r_a + \frac{1}{\alpha} \log \frac{c_+ + c_-}{c_-}$$

and vanishes for

$$r = r_a + \frac{1}{\alpha} \log \frac{c_+ + c_-}{c_-} \quad .$$

Hence, the present treatment confirms the fact that the net charge in the neighborhood of the anode is negative. For values of

$$r > r_a + \frac{1}{\alpha} \log \frac{c_+ + c_-}{c_-}$$

the difference Δ is always positive and so is, therefore, the net charge in that region. Whether the net charge in the entire discharge is positive or negative, depends on the cathode-anode spacing, all other parameters being kept fixed. For example if

$$r_c \leqq r_a + \frac{1}{\alpha} \log \frac{c_+ + c_-}{c_-} \quad ,$$

then obviously $Q < 0$. For very large values of r_c, considering r_a constant, the integral (3-31) becomes positive. Since the integral is a continuous function of r_c, it must vanish at least once.

For higher fields the expression for the drift velocity neglecting inelastic collisions would not be valid anymore. A derivation of an expression for the drift velocity including all types of inelastic collisions has been attempted here

but had to be abandoned because of the too great complexity of the resulting equations. However, it would be possible to lump the inelastic effects into the fractional energy loss χ and then to use for χ a function fitted to the experimental curves which are given in Figure 63 of von Engel (1955). This function can then be substituted into the expression (3-2) for the drift velocity. If both χ_+ and χ_- can be represented by the same function proportional to some power of E/p, say $a\,(E/p)^m$, where a is a constant and m is any positive real number, then the differential equation (3-26) can still be solved by quadrature after the transformation $Y = E^{m + 3/2}$ has been carried out. The assumption of the same functional dependence of χ_+ and χ_- on E/p is however questionable. For while the absolute energy loss suffered by an inelastically colliding electron is the same as that suffered by an inelastically colliding ion (namely the energy difference between the final and initial states of the excited atom), the average energy of the electrons is higher for a given electric field than that of the ions. Hence, the average fractional energy loss of electrons for inelastic collisions is smaller than that of ions. It might be conceivable that the different magnitudes of χ_+ and χ_- can be taken into account by introducing two different coefficients a_+ and a_- with $a_+ > a_-$, while taking the same power m in $(E/p)^m$ for both electrons and ions. This would still leave (3-26) solvable in an elementary way.

However, one should never lose sight of the basic limitation of the entire

treatment which becomes especially severe for higher values of E/p. The expression for the drift velocity used here is based on an "average electron velocity" and therefore completely neglects the electron velocity distribution. The above mentioned phenomenological introduction of a functional dependence of α on E/p should be clearly understood with this in mind. It is actually merely an elementary way of avoiding the real difficulties. A consistent treatment would of course have to start out from the Boltzmann equation.

LIST OF SYMBOLS FOR SECTION IV

$\alpha'_{ff}(\omega)$	effective absorption coefficient
$\alpha_{ff}(\omega)$	absorption coefficient neglecting stimulated emission
K	photon energy, $= \hbar\omega = h\nu$
r_o	classical electron radius, $= \epsilon^2/mc^2$
γ	$\hbar c/\lambda$ Debye
$K_o K_1, K_2$	modified Hankel functions
P_1, P_2	momenta before and after collision, multiplied by c; $\frac{P_1^2}{2\mu} - \frac{P_2^2}{2\mu} = K$
E_1, E_2	energies corresponding to P_1 and P_2; $E_1 - E_2 = K$
μ	mc^2
α	fine structure constant, $= \epsilon^2/\hbar c$
ζ	polarizability of the neutral atom
n_e, n_i, n_a, n_T	densities of electrons, ions, atoms, scatterers
ϵ	electronic charge, to avoid confusion with Naperian base e.
ω_p	plasma angular frequency
ν_c	collision frequency
β_+, β_-	certain sums over atomic quantum numbers, defined in (Barasch et al, 1962)

IV
FREE-FREE ABSORPTION COEFFICIENT IN AN IONIZED GAS

4.1 Introduction

At frequencies exceeding the plasma frequency, the most significant absorption process for electromagnetic radiation in an ionized gas is free-free absorption. In this section we derive the attenuation coefficient corresponding to free-free transitions of the electrons both in the field of singly-charged ions and of neutral atoms or molecules. When the electron density, neutral density, and chemical species are known, these coefficients can be evaluated numerically for a Maxwellian electron distribution of given temperature. They are then found to agree with the attenuation predicted by the classical Lorentz theory (i.e. the limit for zero magnetic field of the Appleton-Hartree relations.) This agreement is to be expected; we shall discuss the point. We also derive the form of the free-free absorption coefficient for non-Maxwellian electron distributions, in terms of the distribution function.

4.2 Principle of Detailed Balance ! Its Utility

The principle of detailed balance states that for a physical system in equilibrium, such as a partially ionized gas, if we focus our attention on a pair of states, (1 and 2) of this system, we will find the rate (number per second) of transitions $1 \rightarrow 2$, T_{12}, equal to the transition rate for $2 \rightarrow 1$, T_{21}. (This is stronger than saying $\sum_i T_{Ki} = \sum_j T_{jK}$). Thus, since cross section for atomic processes are functions

of atomic constants rather than of the gas parameters such as temperature, we may take a situation in which we know just what processes are responsible for the transitions in question, and take a conceptual equilibrium situation. In this equilibrium situation, we can write the transition rates as a function of the cross sections for the processes and their inverses, and by equating the rates, obtain a relation between the cross sections for the processes and for their inverses. Since the cross section is not dependent on the state of the gas, this relation is true out of equilibrium too. Since in most cases the cross section for the inverse process could be obtained directly only by a very laborious quantum-mechanical calculation, the use of detailed balance affords a great saving in effort.

Finally, such things as absorption coefficients, which are a function of the state of the gas, can then be obtained as integrals of these cross sections over the distributions actually existing.

In the present case, we are dealing with transitions between free states of the electron which are separated by microwave frequencies, (free-bound and bound-bound transitions are outside the frequency range of interest) and we know the only operative processes are Bremsstrahlung (spontaneous emission), stimulated emission, and free-free absorption. We shall therefore be able to use detailed balance to relate the cross sections for these three processes, and then formulate the effective absorption coefficient in terms of the previously obtained Bremsstrahlung cross section.

4.3 Some Definitions of Cross Sections and Coefficients for the Relevant Processes; Their Relations to Transition Rates

(a) Bremsstrahlung

The differential cross section for Bremsstrahlung $d\sigma(K, P_1)$ (differential in photon energy K) describes emission of a photon of energy K when the electron originally has $m v_1 c = P_1$, and ends up with P_2 such that $P_1^2 - P_2^2 = 2\mu K$. Let our gas be composed of electrons and massive particles (ions, atoms, or molecules), the latter viewed as existing separately, so we consider cross sections for electron-ion, electron-atom, or electron-molecule interactions with radiation separately. We talk of states of the system (electron + massive particle) and the radiation field. Consider a volume of space V for the whole gas. There are

$$V \left.\frac{dn_e}{dP}\right)_{P_1} dP_1 \, n_T \text{ systems/unit volume}$$

in it with the electron energy in dP_1 at P_1, where n_T is the density of massive particles. Since we take the massive particles as stationary and measure energy from the zero of ionization potential, the energy of the system is the energy of the free electron. Then, at last we may say that the number of Bremsstrahlung transitions per second in a volume of gas V from the continuum range of states with the electron in dP_1 at P_1 and no photon to the range of states with the electron in dP_2 at P_2 and a photon with energy K in dK (where $P_1^2 - P_2^2 = 2\mu K$ and we always consider

dK so small that $P_1 \, dP_1 = P_2 \, dP_2$ may be taken. A non-zero frequency band must be chosen, so that the photon flux within it will be non-zero, but we want to define the cross-sections as nearly at a single frequency as possible) is given by

$$T^1_{P_1 \to P_2} = n_T \left(\frac{dn_e}{dP} \right)_{P_1} V \, dP_1 \, v_1 \, d\sigma_{BR}(K, P_1) \qquad (4\text{-}1)$$

(b) Free-Free Absorption

Let I(K) be the spectral density of radiation flux at photon energy $K = \hbar\omega$, so that the flux in dK is I(K) dK. The macroscopic law to which we want the absorption coefficient α_{ABS} and cross section σ_{ABS} to correspond to is

$$d\,I(K) = -I(K)\,\alpha(K)\,dx\,. \qquad (4\text{-}2)$$

In the case where absorption of radiation of frequency ω in a narrow band $d\omega$ takes place by systems in the range dP_2 at P_2, raising them to dP_1 at P_1 such that $P_1^2 - P_2^2 = 2K\mu$, and $P_1 \, dP_1 = P_2 \, dP_2$

$$d\left[I(K)dK\right] = -\left[I(K)dK\right] \left(\frac{dn_{systems}}{dP} \right)_{P_2} dP_2 \, \sigma_{ABS}(K, P_2)\, dx\,. \qquad (4\text{-}3)$$

Now consider a rectangular volume of length dx traversed by this radiation, with area A normal to it. Clearly the number of events/sec in V = A dx is

$$T^2_{P_2 \to P_1} = \frac{\text{energy loss in V/sec}}{\text{energy/photon}} = \frac{A\,dx\,I(K)\,dK}{K} \left.\frac{dn}{dP}\right)_{P_2} dP_2 \sigma_{ABS}(K,\ P_2)\ , \tag{4-4}$$

$$= \frac{I(K)dK}{K} \left.\frac{dn}{dP}\right)_{P_2} dP_2\, \sigma_{ABS}(K,\ P_2)\ V \quad . \tag{4-5}$$

Finally, we put $I(K)\,dK$ in terms of the volume density of photons $n_{PHOT}(K)dK = \frac{I(K)dK}{Kc}$, and replace the system distribution by the electron distribution multiplied by $n_T V$, since the massive particles are stationary. Thus, we write to define $\sigma_{ABS}(K,\ P_2)$,

$$T^2_{P_2 \to P_1} = n_{PHOT}(K)dK\ cV \left.\frac{dn_e}{dP}\right)_{P_2} dP_2\ \sigma_{ABS}(K,\ P_2)\, n_T V\ . \tag{4-6}$$

We also note for later use that the differential absorption coefficient (differential in electron energy), is

$$d\alpha_{ABS}(K) = dn_e(P_2)\sigma_{ABS}(K,\ P_2)\ . \tag{4-7}$$

(c) Stimulated Emission

This process goes from the ranges dP_1 at P_1 down to dP_2 at P_2, but is governed by the same law as free-free absorption. We therefore write down

immediately

$$T^3_{P_1 \to P_2} = n_{PHOT}(K)dKc\ V \left.\frac{dn_e}{dP}\right)_{P_1} dP_1\, \sigma_{S.\ EM}(K,\ P_1) n_T V \qquad (4\text{-}8)$$

with the relation

$$d\alpha_{S.\ EM} = dn_e(P_1)\, \sigma_{S.\ EM}(K,\ P_1)\ . \qquad (4\text{-}9)$$

4.4 Degeneracies

Detailed balance deals with transition rates between states, not ranges. Since our probabilities are the same for all states in the ranges, it is evident that the transition rates between a pair of states, R_i, are obtained by dividing the T^i by the products of the numbers of initial and final states of the electron-massive system and the radiation field (i.e. the degeneracies). These reflect the fact that our cross sections refer to $|P|$ and $|K|$ rather than $\vec{P}$ and photon propagation direction, and include neither electron spin nor photon polarization, so that many states correspond to a "condition" $|P|$ in dP, $|K|$ in dK. Detailed balance will then state that $R_1 + R_2 = R_3$, where

$$R_1 = \frac{\left.n_T \frac{dn_e}{dP}\right)_{P_1} dP_1\, v_1\, d\sigma_{Br}(K,\ P_1)\, V}{\left[\frac{8\pi P_2^2}{(hc)^3} dP_2\, V\right]\left[V\frac{8\pi K^2 dK}{(hc)^3}\right]\left[V\frac{8\pi P_1^2 dP_1}{(hc)^3}\right]} \qquad (4\text{-}10)$$

$$R_2 = \frac{n_{PHOT}(K)dK\, C \left(\frac{dn_e}{dP_2}\right)_{P_2} dP_2\, \sigma_{ABS}(K, P_2) V\, n_T\, V}{\left[V\frac{8\pi P_1^2}{(hc)^3}\, dP_1\right]\left[V\frac{8\pi K^2 dK}{(hc)^3}\right]\left[V\frac{8\pi P_2^2\, dP_2}{(hc)^3}\right]} \qquad (4\text{-}11)$$

$$R_3 = \frac{n_{PHOT}(K)\, dK\, C \left(\frac{dn_e}{dP}\right)_{P_1} dP_1\, \sigma_{S.EM}(K, P_1)\, V\, n_T\, V}{\left[V\frac{8\pi P_2^2}{(hc)^3}\, dP_2\right]\left[V\frac{8\pi K^2 dK}{(hc)^3}\right]\left[V\frac{8\pi P_1^2\, dP_1}{(hc)^3}\right]} \; . \qquad (4\text{-}12)$$

We see now that there is no way of avoiding the usual choice $n_T V = 1$, i.e., we must work in an "atomic volume". Such a volume has in it on the average $n_e n_T^{-1}$ systems, which is < 1 for us when the massive particles are neutrals in a weakly ionized gas, so that the situation is unsatisfactory, fluctuations about the average being then relatively important. This is the same situation as met in the derivation of the Saha equation, and, as is customary, we adopt the procedure without further comment.

4.5 Relation between σ_{ABS} and $\sigma_{S.EM}$

Although it does not evaluate these cross sections explicitly, quantum mechanics indicates that they are related. For the a priori transition rates per system between a pair of states (that is, removing the weighting by occupation

probability) are equal for free-free absorption and stimulated emission. (See Schiff , 1949). We therefore take (4-11) and (4-12), remove from each the statistical weighting factor $e^{-P_1^2/2\mu kT}$ implicit in the $\left(\frac{dn_e}{dP}\right)_{P_i}$, and equate them. The resulting relation is

$$P_1 P_2^2 \sigma_{ABS}(K, P_2) = P_2 P_1^2 \sigma_{S.EM}(K, P_1) \tag{4-13}$$

or

$$P_2 \sigma_{ABS}(K, P_2) = P_1 \sigma_{S.EM}(K, P_1) \tag{4-14}$$

4.6 Relations in Equilibrium

The statement of detailed balance is

$$R_1 + R_3 = R_2 \tag{4-15}$$

Using (4-14) and the fact that in equilibrium,

$$n_{PHOT}(K)\, dK = \frac{8\pi K^2 dK}{(hc)^3 (e^{K/kT} - 1)} , \tag{4-16}$$

while

$$\left(\frac{dn_e}{dP}\right)_{P_i} dP_i = \frac{n_e 4\pi P_i^2 e^{-P_1^2/2\mu kT}}{(2\pi \mu kT)^{3/2}} dP_i , \tag{4-17}$$

we obtain

$$\sigma_{ABS}(K, P_2) = \frac{n_T P_1^2 (hc)^3}{\mu P_2 8\pi K^2} \frac{d\sigma_{Br}}{dK}(K, P_1) \cdot \tag{4-18}$$

We also obtain

$$\sigma_{S.EM}(K, P_1) = \frac{n_T P_1 (hc)^3}{\mu \cdot 8\pi K^2} \frac{d\sigma_{Br}}{dK}(K, P_1) . \tag{4-19}$$

Both (4-18) and (4-19), although obtained by detailed balance (i.e. in equilibrium), are true in general. However, relations between absorption coefficients depend on the state of the gas, and are not general. Let us first attempt to verify the relation which is known to hold in equilibrium between the effective absorption coefficient and that neglecting stimulated emission.

We have the definition

$$\alpha'_{ff}(K) = \int dn_e(P) \left[\sigma_{ABS}(K, P_2) - \sigma_{S.EM}(K, P_1)\right] , \tag{4-20}$$

where in the first term the integration is over the initial P for absorption, P_2, and the lower limit is therefore $P_2 = 0$. In the second term, the initial P is P_1, but since a photon of energy K can be emitted only by an electron of energy $\frac{P_1^2}{2\mu} \geq K$, the lower limit is $P_1 = \sqrt{2 K \mu}$. Thus

$$\alpha'_{ff}(K) = n_e \int_0^\infty dP_2 \frac{4\pi P_2^2 \, e^{-P_2^2/2\mu kT}}{(2\pi \mu kT)^{3/2}} \sigma_{ABS}(K, P_2)$$

$$- n_e \int_{\sqrt{2K\mu}}^\infty dP_1 \frac{4\pi P_1 P_2 \, e^{-P_1^2/2\mu kT}}{(2\pi \mu kT)^{3/2}} \sigma_{ABS}(K, P_2) \quad , \tag{4-21}$$

where we have employed (4-14) in the second integral. But since K is fixed, we find from conservation of energy (which is $P_1^2 = P_2^2 + 2K\mu$) that

$$P_1 \, dP_1 = P_2 \, dP_2 \quad . \tag{4-22}$$

We use this to transform the second integration to one over P_2, and obtain

$$\alpha'_{ff}(K) = n_e \int_0^\infty dP_2 \frac{4\pi P_2^2}{(2\pi \mu kT)^{3/2}} \sigma_{ABS}(K, P_2) \, e^{-P_2^2/2\mu kT} \left[1 - e^{-K/kT}\right] \tag{4-23}$$

Now, of course, α_{ff} is the absorption coefficient which would have been obtained by neglecting stimulated emission, or

$$\alpha_{ff}(K) = n_e \int_0^\infty dP_2 \frac{4\pi P_2^2 \, e^{-P_2^2/2\mu kT}}{(2\pi \mu kT)^{3/2}} \sigma_{ABS}(K, P_2) \quad . \tag{4-24}$$

We have verified, then, by combining (4-23) and (4-24), that in equilibrium

$$\alpha'_{ff}(K) = (1 - e^{-\hbar\omega/kT})\,\alpha_{ff}(K) \quad . \tag{4-25}$$

In equilibrium, the explicit relation given by detailed balance between $\alpha'_{ff}(K)$ and $\frac{d\sigma_{Br}}{dK}(K, P_1)$, obtained by combining (4-18) and (4-23), with a change to integrating over P_1 is,

$$\alpha'_{ff}(K) = \frac{n_e n_T (hc)^3 (e^{K/kT} - 1)}{2K^2\mu\,(2\pi\,\mu kT)^{3/2}} \int_{\sqrt{2K\mu}}^{\infty} dP_1\, P_1^3\, e^{-P_1^2/2\mu kT} \frac{d\sigma_{Br}}{dK}(K, P_1) \quad . \tag{4-26}$$

We use this when $\frac{d\sigma_{Br}}{dK}(K, P_1)$ is possible to formulate by a direct procedure, but α'_{ff} would be tedious to obtain by finding σ_{ABS} and $\sigma_{S.EM}$ directly. If $\frac{d\sigma_{Br}}{dK}(K, P_1)$ is given as a function of both P_1 and P_2, P_2 is to be eliminated by expressing it as $\sqrt{P_1^2 - 2K\mu}$.

4.7 Absorption Coefficient out of Equilibrium

The relations (4-18) and (4-19), which are valid in general, are the starting points, to be inserted into (4-20). The result is

$$\alpha'_{ff}(K, \vec{r}) = \frac{n_T (hc)^3}{8\pi K^2 \mu} \left[\int_0^\infty dn_e (P_2, \vec{r}) \frac{P_1^2}{P_2} \frac{d\sigma_{Br}}{dK} (K, P_1) \right.$$

$$\left. - \int_{\sqrt{2K\mu}}^\infty dn_e (P_1, \vec{r}) P_1 \frac{d\sigma_{BR}}{dK} (K, P_1) \right] \qquad (4\text{-}27)$$

wherein conservation of energy is to be used to eliminate P_1 in the first integral. The use of the symbol $\vec{r}$ indicates the possibility of a spatially inhomogeneous electron distribution.

It must be admitted that this equation is of limited utility, since in a non-equilibrium situation, the form of dn_e may depend on the spectral density of radiation present. However, in many practical situations, applied potential gradients or temperature gradients rather than externally generated electromagnetic energy are the essential factors in determining dn_e, which may then be obtained separately and inserted into (4-27) to give a meaningful result.

4.8 Summary of Expressions for the Bremsstrahlung Cross-Section

The effective attenuation coefficient due to free-free transitions may be evaluated if the Bremsstrahlung cross-section $\frac{d\sigma_{BR}}{dK}(K, P_1)$ is known. In work under other contracts, expressions for this quantity have been obtained, which

pertain to Bremsstrahlung in the fields of ions, atoms, and molecules respectively. We shall now list them.

In the field of singly-charged ions, we use (Barasch, 1960) separate expressions for the faster and slower electrons. For the faster ones,

$$\frac{d\sigma_{BR}}{dK}(K,P_1)=\frac{16}{3}\frac{\alpha r_o^2 \mu^2}{P_1^2 K}\left[\frac{1}{2}\ln\frac{(P_1+P_2)^2+\gamma^2}{(P_1-P_2)^2+\gamma^2}-\frac{2\gamma^2 P_1 P_2}{[(P_1+P_2)^2+\gamma^2][(P_1-P_2)^2+\gamma^2]}\right], \tag{4-29}$$

while for the slower ones,

$$\frac{d\sigma_{BR}}{dK}(K,P_1)=\frac{16}{3}\frac{\alpha r_o^2 \mu^2}{P_1^2 K}\left\{\sqrt{\left(\frac{\gamma}{P_1}\right)^2+\left(\frac{\mu K}{P_1^2}\right)^2}\;K_o(\sqrt{\;})K_1(\sqrt{\;})-\right.$$

$$\left.-\frac{1}{2}\left[\left(\frac{\gamma}{P_1}\right)^2+2\left(\frac{\mu K}{P_1^2}\right)^2\right]\left[K_1^2(\sqrt{\;})-K_o^2(\sqrt{\;})\right]\right\} \tag{4-30}$$

where the symbol $\sqrt{\;}$ denotes the first square root written explicitly.

The criterion for distinguishing between fast and slow electrons is essentially that $P_1 > P_{1C}$, where $\alpha\mu\left[\frac{1}{P_2}-\frac{1}{P_{1C}}\right] << 1$, and where $P_{1C}^2 = P_2^2 + 2K\mu$. We often find a choice of $P_{1C}=\sqrt{\mu k T}$ to be satisfactory and to simplify the subsequent integrations.

In the field of neutral atoms, the Bremsstrahlung is treated by the method of Heitler, using a Hamiltonian which includes all Coulomb interactions and the

radiation field. The result (Barasch et al, 1962) contains two contributions, the first of which arises from the static potential of the atom and the second from the polarizability. The second should be negligible for situations of practical interest, so we write them separately and neglect the interference between them which is indicated by the formalism. The static contribution is

$$\frac{d\sigma_{BR}}{dK}(K, E_1) = \frac{4}{3\pi} \frac{\alpha\sigma(o) E_1}{K\mu} (2 - K/E_1) \sqrt{1 - K/E_1} \qquad (4\text{-}31)$$

Here $\sigma(o)$ is the elastic scattering cross-section of the neutral atom, for low-energy electrons and E_1 is the energy of the incident electrons, or $E_1 = P_1^2/2\mu$.

The contribution due to polarizability of the neutral atom is (Barasch et al, 1962)

$$\frac{d\sigma_{BR}}{dK}(K, E_1) = \frac{8}{3} \frac{\alpha\mu}{(\hbar c)^4} \frac{K^3}{E_1} \left[\xi^2 + 2(\beta_+^2 + \beta_-^2) \right] \ln \left[\frac{1 + \sqrt{1 - K/E_1}}{1 - \sqrt{1 - K/E_1}} \right] . \qquad (4\text{-}32)$$

Finally, for neutral molecules, an expression identical to (4-31) was obtained, except that $\sigma(o)$ is now the scattering cross-section of the molecule for slow electrons. Thus, again,

$$\frac{d\sigma_{BR}}{dK}(K, E_1) = \frac{4\alpha\sigma(o) E_1}{3\pi K\mu} (2 - K/E_1) \sqrt{1 - K/E_1} . \qquad (4\text{-}33)$$

4.9 Corresponding Expressions for the Effective Free-free Absorption Coefficient

We shall give the explicit forms assumed in equilibrium by the effective absorption coefficient corresponding to these Bremsstrahlung cross-sections. The starting point is equation (4-26),

$$\alpha'_{ff}(K) = \frac{n_e n_T (hc)^3 (e^{K/kT} - 1)}{2K^2 \mu (2\pi\mu kT)^{3/2}} \int_{\sqrt{2K\mu}}^{\infty} dP_1 \, P_1^3 \, e^{-P_1^2/2\mu kT} \frac{d\sigma_{BR}}{dK}(K, P_1) .$$

Consider first the free-free absorption in the field of ions. The integration over the lower-velocity part of the electron distribution must be performed numerically, and that over the faster ones depends, of course, on the value of P_1 chosen as the division between slow and fast. If we choose, for example, the lower limit of integration as $P_1 = \sqrt{\mu kT}$, and find that the approximations $P_1 + P_2 \gg \gamma$, $P_1 \sim P_2$ are valid, and also use the relation $P_1 - P_2 = \frac{2K\mu}{P_1 + P_2}$, we find for the contribution of the faster electrons

$$\alpha'(\omega) = \frac{4\sqrt{2}\, n_e}{3\pi}\left(\frac{\omega_p}{\omega}\right)^2 \mu\epsilon^4 \left(\frac{\pi}{\mu kT}\right)^{3/2} \left\{ -\mathrm{Ei}(-1/2) - \frac{1}{2\sqrt{e}} - \frac{1}{2\sqrt{e}} \ln\left[\left(\frac{\hbar\omega}{kT}\right)^2 + \left(\frac{\hbar\omega_p}{kT}\right)^2\right] \right.$$

$$\left. - \frac{1}{2} \exp\left[\frac{1}{2}\omega^2/\omega_p^2\right] \mathrm{Ei}\left(-1/2 - 1/2\, \omega^2/\omega_p^2\right) \right\} \qquad (4\text{-}34)$$

For the static contribution to free-free absorption in the field of neutral atoms, insertion of equation (4-31) into equation (4-26) and changing the variable of integration to E_2 yields

$$\alpha'(\omega) = \frac{32\sqrt{\pi}\, n_a n_e \alpha\sigma(o)}{3\omega^3 (mkT)^{3/2}} \frac{\hbar\omega}{kT} \int_0^\infty dE\, E^{1/2} (E+\hbar\omega)^{1/2} (E+\frac{\hbar\omega}{2})\, e^{-E/kT}\,, \qquad (4\text{-}35)$$

where we have already taken $\hbar\omega/kT << 1$, so that $1 - e^{-\hbar\omega/kT} \approx \hbar\omega/kT$.

We employ a change of variable to $y = E/\hbar\omega$, split the integral into two terms resulting from the factor $E + \frac{\hbar\omega}{2}$, and obtain integrals which are evaluated in terms of the function $K_1(x)$ and its derivative. Recurrence relations on this function are then used to convert this result to a $K_2(x)$. That is,

$$\alpha'(\omega) = \frac{32\sqrt{\pi}\, n_a n_e \alpha\sigma(o)}{3\omega^3 (mkT)^{3/2}} \frac{\hbar\omega}{kT} (\hbar\omega)^3 \left[\int_0^\infty y\, dy \sqrt{y(y+1)}\, e^{-sy} + \right.$$

$$\left. + \frac{1}{2} \int_0^\infty dy \sqrt{y(y+1)}\, e^{-sy} \right]\,, \qquad (4\text{-}36)$$

where $s = \hbar\omega/2kT$. Then

$$\alpha'(\omega) = A(\omega, T)\left[\frac{1}{4s}\, e^{s/2} K_1(s/2) - \frac{\partial}{\partial s}\left(\frac{1}{2s}\, e^{s/2} K_1(s/2)\right)\right]$$

$$= A(\omega, T)\left[\frac{1}{8t}\, e^{t} K_1(t) - \frac{1}{2}\,\frac{\partial}{\partial t}\left(\frac{1}{4t}\, e^{t} K_1(t)\right)\right] \quad , \text{ where } t = s/2$$

$$= A(\omega, T)\left[\frac{e^t}{8t} K_1(t) + \frac{e^t}{8t^2} K_1(t) + \frac{e^t}{16t}\left(K_o(t) + K_2(t)\right)\right]$$

$$= A(\omega, T)\left[\frac{K_1(t)}{t} + \frac{1}{2}(K_o + K_2)\right]\frac{e^t}{8t}$$

$$= A(\omega, T)\,\frac{e^t}{8t} K_2(t)$$

$$= \frac{8\sqrt{\pi}\, n_a n_e \alpha\, \sigma/o)\, \hbar^3}{3\,(mkT)^{3/2}}\; e^{h\omega/2kT}\; K_2\left(\frac{\hbar\omega}{2kT}\right) \quad . \tag{4-37}$$

Now for $\hbar\omega/2kT << 1$, $K_2\left(\frac{\hbar\omega}{2kT}\right) \to 8\left(\frac{kT}{\hbar\omega}\right)^2$, so finally we may write

$$\alpha'_{\text{static}}(\omega) \cong \frac{64\sqrt{\pi}\, n_a n_e \alpha\, \sigma(o)\, \hbar\, (kT)^{1/2}}{3\,\omega^2\, m^{3/2}} \tag{4-38}$$

For the contribution of the induced dipole in the neutral atom, we insert equation (4-32) into equation (4-26). Thus,

$$\alpha'_{\text{dipole}}(\omega)=\frac{16\sqrt{2}\,\pi^{3/2}\omega n_a n_e}{3\left(\frac{kT}{m}\right)^{1/2}kT}\,\alpha\left[\zeta^2+2(\beta_+^2+\beta_-^2)\right]\,(e^{\hbar\omega/kT}-1)\int_K^\infty dE_1\, e^{-E_1/kT}\cdot$$

$$\cdot\ \ln\left[\frac{1+\sqrt{1-K/E_1}}{1-\sqrt{1-K/E_1}}\right]\cdot \qquad (4\text{-}39)$$

Rationalizing the denominator of the argument of the logarithm, we may write the integral as

$$I_1 = 2\int_K^\infty d\,E_1\, e^{-E_1/kT}\ln\left[\sqrt{\frac{E_1}{K}}+\sqrt{\frac{E_1}{K}-1}\right]. \qquad (4\text{-}40)$$

We now introduce the substitution

$$x = \frac{1}{2}\cosh^{-1}\sqrt{E_1/K} \qquad (4\text{-}41)$$

and obtain the relation

$$I_1 = 2kT\int_0^\infty dx\, e^{-\hbar\omega\cosh^2 x/kT} = kT\, e^{-\hbar\omega/2kT}\int_0^\infty d\,y\, e^{-\frac{\hbar\omega}{2kT}\cosh y}$$

$$= kT\, e^{-\hbar\omega/2kT}\, K_o(\hbar\omega/2kT)\ . \qquad (4\text{-}42)$$

Thus the contribution is given by

$$\alpha'_{\text{dipole}}(\omega) = \frac{16\sqrt{2}\,\pi}{3}\left(\frac{m\pi}{kT}\right)^{1/2} n_a n_e \alpha\left[\zeta^2+2(\beta_+^2+\beta_-^2)\right]\omega\, e^{\frac{\hbar\omega}{2kT}}$$

$$(1-e^{-\hbar\omega/kT})\,K_o\left(\frac{\hbar\omega}{2kT}\right)\ . \qquad (4\text{-}43)$$

We note further that since $\lim_{x \to o} K_o(x) = -\ell n\,(x/2)$, we have for $\hbar\omega/kT \to o$ that $\alpha'_{dipole}(\omega)$ vanishes as ω^2, or

$$\lim_{\omega \to o} \alpha'_{dipole}(\omega) = \frac{8\sqrt{2}\,\pi}{3}\left(\frac{m\pi}{kT}\right)^{1/2} n_a n_e \alpha \left[\zeta^2 + 2\,(\beta_+^2 + \beta_-^2)\right] \frac{\hbar\omega^2}{kT} \quad . \tag{4-44}$$

The ratio of this value to the limit for small $\hbar\omega/kT$ of the static contribution is

$$\lim_{\frac{k\omega}{kT} \to 0} \frac{\alpha'_{dipole}(\omega)}{\alpha'_{static}(\omega)} = \frac{1}{8}\left(\frac{m\,\omega^2}{kT}\right)^2 \left[\frac{\zeta^2 + 2\,(\beta_+^2 + \beta_-^2}{\sigma(0)}\right] \quad . \tag{4-45}$$

As an example, consider a closed-shell atom, for which $\beta_+ = \beta_- = 0$. Then $\zeta \sim 10^{-24}$ cm^3 (Firsov and Chibisov, 1960), while usually $\sigma(0) \sim 10^{-16}$ cm^2. Thus even for the highest frequencies we might consider, the dipole contribution to free-free absorption may be neglected with respect to the static potential effect.

Since the Bremsstrahlung cross-section for the molecule had the same form as that for the neutral atom in our approximation, we may write immediately for the free-free absorption coefficient in the field of molecules

$$\alpha'_{molecule} \cong \frac{64\sqrt{\pi}\, n_a n_e \alpha \sigma(0)\, \hbar\, (kT)^{1/2}}{3\,\omega^2\, m^{3/2}} \quad . \tag{4-46}$$

4.10 Relation to the Lorentz Formulation

The interaction between radiation and an ionized gas is phenomenologically described by the coefficients of absorption and emission, or alternately by the electrical conductivity. The alternate use of these coefficients tends to obscure the fact that all of them are manifestations of the same atomic mechanisms. The mechanism pre-eminent in the radio-frequency range is free-free transitions. (Paraphrase of introductory remarks of Oster, 1961).

This discussion refers to the situation of operation at frequencies above the plasma frequency, where at least the classical description, upon which most engineers' intuition is based, attributes attenuation to the dissipative effect of collisions. That is, the Lorentz attenuation coefficient (i.e. the $\vec{H} = 0$ case of the Appleton-Hartree equations) vanishes for vanishing collision frequency. It is clear that our quantum-mechanical approach is describing the same process as the collisional dissipation in the Lorentz treatment. Their numerical predictions should then agree well to the accuracy of the approximations inherent in both procedures, and their dependence on ω, T, n_e and ν should be closely related.

The good numerical agreement has been verified in a number of calculations which were made on classified problems and submitted to ARPA and AFCRL, the sponsoring agencies for this contract. In order to preserve the unclassified status of this report, we shall not reproduce them here. It is of interest, however, to compare the functional form of the attenuations in the two approaches.

After some manipulation, the absorption coefficient for free-free transitions in the static field of neutral atoms (equation 4-38) may be written

$$\alpha'_{ff}(\omega) = \frac{4\sqrt{2}}{3}\,\frac{\nu_c}{c}\left(\frac{\omega_p}{\omega}\right)^2, \tag{4-47}$$

where we have defined $\nu_c = n_a\left(\frac{8kT}{\pi m}\right)^{1/2}\sigma(0)$ as the collision frequency, and introduced $\omega_p^2 = \frac{4\pi n_e e^2}{m}$.

Correspondingly, the power attenuation coefficient from the Lorentz expression is approximated to order $\left(\frac{\omega_p}{\omega}\right)^2$ by the expression

$$\alpha_L(\omega) = \frac{\nu_c}{c}\left(\omega_p/\omega\right)^2 \tag{4-48}$$

when $\left(\frac{\nu_c}{\omega}\right)^2 << 1$ also. Now we expect that collisional dissipation or free-free absorption should be the predominant process only a bit above the plasma frequency, since a resonance may exist there. Thus, it is reasonable to use the two expressions only for, roughly, $\omega_p/\omega < 1/3$. Since the next term in the expansion of the Lorentz equation is of order $\left(\omega_p/\omega\right)^4$, it is justified to use the approximate form (4-48) in the joint region of validity of both approaches. The restriction on collision frequency is related to the averaging process employed in the derivation of the Lorentz equations; it must be meaningful to speak of the electron as between collisions during a cycle, and collisions should not overlap each other. An uncertainty principle argument which demands that the relative uncertainty in photon

energy be $\ll 1$, and relates this to uncertainties in electron energy corresponding to measuring this within a Δt= mean free time, $1/\nu_c$, yields the same restriction on ν/ω for the quantum-mechanical case. We thus conclude that for the regimes in which both expressions may safely be used, they have the same functional dependence, and agree to within a factor of $\frac{4\sqrt{2}}{3} \sim 1.9$. This factor could be a result of improper averaging in the Lorentz derivation, or an inaccuracy of the perturbation theory used to derive the quantum-mechanical result. In any case, both formulas are clearly talking about the same thing.

For the case of electron-ion interaction, a collision frequency to be inserted into the Lorentz equation is given by (Shkarofsky, 1961). It is, in our notation,

$$\langle \nu_{ei} \rangle = \frac{4\sqrt{2\pi}}{3} n_e \left(\frac{\epsilon^2}{kT}\right)^2 \left(\frac{kT}{m}\right)^{1/2} \ln\left[\frac{3}{2\sqrt{\pi n_e}} \left(\frac{kT}{\epsilon^2}\right)^{3/2}\right] . \qquad (4\text{-}49)$$

Computations using this expression agree well with those using our relation (4-34). The functional dependence is the same, except for the $\ln$ here replacing our sum of terms inside the bracket. For parameters we have used, these correction factors differ little.

Attenuation processes below and in the immediate neighborhood of the plasma frequency have not been studied; the following statements are thus conjectural. Intuition based on the Lorentz treatment suggests that attenuation

below the plasma frequency is purely reactive and non-zero for a collisionless plasma, and not linearly dependent on collision frequency when this quantity is introduced (Ratcliffe, 1959). Free-free absorption by uncorrelated events is probably not the correct picture here, and we suspect that the Lorentz equations could be in error, too. An investigation based on the microfield in a plasma, as well as the classical or quantum-mechanical dynamics of the collisions, seems to be the appropriate approach.

V

CONCLUSIONS

An investigation, both theoretical and experimental, has been initiated into the absorption of electromagnetic radiation by a plasma at frequencies exceeding the plasma frequency.

The theoretical work has concentrated on free-free absorption rather than on any resonant effects that may occur in the immediate vicinity of the plasma frequency. Expressions have been obtained for the free-free absorption coefficient in the presence of both ions and neutral particles. These expressions are evaluated explicitly for the case of a Maxwellian electron distribution, and given in terms of integrals over the distribution function for non-equilibrium situations. In the latter case, since the distribution function depends in principle on the spectral density of radiation present and the absorption coefficient, the solution is purely formal. However, it may be used in situations for which the distribution function is primarily determined by such effects as thermal gradients or potential gradients rather than by interaction with incident radiation.

The experimental investigation has obtained data for the interaction of radiation with a pure electron stream. A simple physical model based on Lorentz theory and introducing a collision frequency with the walls succeeds only partially in accounting for the data. In particular, the absorption of radiation by the

electron stream in the vicinity of the plasma frequency is not explained satisfactorily as yet. Attempts to introduce gases such as helium have caused cathode poisoning due to impurities evolving in the system at a rate more rapid than expected. For this reason the data obtained on helium from the first cathode was not sufficiently reliable to warrant analysis. Time did not permit helium runs.

In order to interpret the experimental results it is necessary to know the electron distribution within the tube. A considerable effort has been devoted to this problem, with the results to date presented here.

The theoretical investigation of free-free absorption led to the conclusion that for frequencies reasonably above the plasma frequency, the classical Lorentz approach predicts the attenuation with satisfactory accuracy, or more precisely, agrees well with the free-free absorption coefficient. It was hoped that the experimental results would provide a check on the theoretical work, to permit a decision on whether the theoretical results are both correct, or merely consistent but in error because of the neglect of other attenuation mechanisms. This hope has not yet been completely realized, and we feel that the experiments required should be performed.

We also have serious doubts concerning the validity of the Lorentz equations below the plasma frequency, and feel strongly that experimental and

theoretical work in this area should be initiated, as should a study of the immediate neighborhood of the plasma frequency, where the interplay of several phenomena creates a complex situation.

ACKNOWLEDGEMENT

The authors would like to thank Professor Keeve M. Siegel and Mr. Ralph E. Hiatt for their advice and support in the course of this investigation. A debt is owed to Professor S. Silver, Dr. R. F. Goodrich, Dr. G. Owyang, and Dr. D. L. Sengupta for many suggestions. The advice of B. Wolk (Sylvania Research Lab., Bayside, L. I., NY), G. Becker (Electronics Research Lab., U of Calif., Berkeley), V. R. Burris and L. E. Paul (Electron Physics Lab., U of Mich), on the problems of technology was indispensible. We wish to express our appreciation to E. Rupke for his assistance on many mechanical problems associated with the experiment; to G. McIlvain and K. Young for their help in carrying out the experiment, and to Z. A. Akcasu for his work on the problem of free-free absorption.

APPENDIX A

A VARIATIONAL DETERMINATION OF THE PROPAGATION CONSTANT IN AN INHOMOGENOUS COAXIAL LINE

This appendix is concerned with the propagation characteristics of a coaxial wave guide which is filled with a dielectric substance whose permittivity varies only radially. At present we shall discuss an averaging procedure which will enable us to take into account the variable nature of the dielectric substance. Ultimately, it is hoped that a perturbation procedure may be derived which will enable us to correct this averaging method in order to give a more detailed account of the presence of the dielectric.

We consider first a coaxial wave guide which is filled with a dielectric of permittivity $\epsilon = \epsilon(r)$, and a constant permeability μ_o. With the time dependence assumed to be $\exp(j\omega t)$, the components of the electric and magnetic fields may be derived from the vector potential $\bar{\pi}$ by the following relations

$$\bar{H} = j\omega \nabla \times (\epsilon \bar{\pi})$$

and

$$\bar{E} = 1/\epsilon \nabla \times \nabla \times (\epsilon \pi)$$

If we take $\bar{\pi}$ to depend on a single component, that is $\bar{\pi} = i_z \pi_z$, we have

$$\nabla^2 \epsilon \pi_z + \mu_o \omega^2 \epsilon^2 \pi_z = 0 \quad . \tag{A-1}$$

From the expressions $\bar{E}$ and $\bar{H}$ we may calculate the explicit forms of the components in terms of π_z, that is,

$$\epsilon E_r = \frac{1}{r} \frac{\partial}{\partial r} r \frac{\partial}{\partial r} \epsilon \pi_z = \frac{\partial^2}{\partial z \partial r} \epsilon \pi_z,$$

$$\epsilon E_\phi = \frac{1}{r} \frac{\partial^2}{\partial z \partial \phi} \epsilon \pi_z,$$

$$\epsilon E_z = -\frac{1}{r} \left[\frac{\partial}{\partial r} r \frac{\partial}{\partial r} \epsilon \pi_z + \frac{1}{r} \frac{\partial^2}{\partial \phi^2} \epsilon \pi_z \right]$$

$$= \frac{\partial^2}{\partial z^2} \epsilon \pi_z + \omega^2 \epsilon^2 \mu_o \pi_z,$$

$$H_r = \frac{j\omega}{r} \frac{\partial}{\partial \phi} \epsilon \pi_z,$$

$$H_\phi = -j\omega \frac{\partial}{\partial r} \epsilon \pi_z$$

and

$$H_z = 0$$

where the coordinates r, ϕ, z are the customary cylindrical coordinates. The above fields are divergence free, that is

$$\nabla \cdot (\mu_o \bar{H}) = 0$$

and

$$\nabla \cdot (\epsilon E) = 0$$

Furthermore, these components describe an E type of field, there being no need of an H type of field since we shall require excitation in terms of the principal mode.

Since we shall ultimately be concerned with an excitation which is axially symmetric, that is independent of the angle ϕ, the field components which we just described assume the form

$$\epsilon E_r = \frac{\partial^2}{\partial z \partial r} \epsilon \pi_z,$$

$$\epsilon E_z = -\frac{1}{r} \frac{\partial}{\partial r} r \frac{\partial}{\partial r} \epsilon \pi_z = \frac{\partial^2}{\partial z^2} \epsilon \pi_z + \omega^2 \epsilon^2 \mu_o \pi_z$$

$$H_\phi = -j\omega \frac{\partial}{\partial r} \epsilon \pi_z$$

and

$$E_\phi = H_r = H_z = 0 \quad .$$

Consider now a coaxial wave guide of inner radius a and outer radius b with perfectly conducting walls. On these walls we have the boundary conditions $E_z(a, z) = E_z(b, z) = 0$. The presence of the variable permittivity $\epsilon = \epsilon(r)$ complicates the formation of solutions of equation (A-1), from two points of view. That is, the ϵ is contained both in the differential equation as well as in the boundary condition. In order to circumvent this difficulty, we note that we can write separated solutions of (A-1) in the form

$$\epsilon \pi_z = \exp(j\alpha z)\, f(r).$$

From this we find that $f(r)$ satisfies the ordinary linear differential equation

$$\frac{1}{r}\,\frac{d}{dr}\, r\,\frac{df}{dr} + (\mu_o \omega^2 \epsilon^2 - \alpha^2) f = 0 \qquad \text{(A-2)}$$

and (A-2) is to be solved subject to the boundary conditions $f(a) = f(b) = 0$.

Now we are in a position to describe a variation principle for determining the smallest characteristic value α. That is, we have an effective method of finding the smallest characteristic value α of equation (A-2) solved subject to the boundary conditions which are imposed by the problem. Indeed, upon multiplying equation (A-2) through by $rf(r)$, integrating by parts and noting the boundary conditions, we get

$$\frac{\int_a^b \left[\mu_o \omega^2 \epsilon^2(r)\, r\, f^2(r) - r f'^2(r)\right] dr}{\int_a^b r f^2\, dr} = \alpha^2$$

and for the class of admissable functions f, α is above a minimum α_o. α_o will be a minimum for the correct function f.

APPENDIX B

APPROXIMATE EVALUATION OF THE INTEGRAL $\int_{\xi}^{\xi_c} e^{\frac{3}{2}x_1^2} dx_1$

The simplest method is, of course, the power series expansion of the integrand followed by term by term integration. Whenever the exponent (i.e., the upper limit of the exponent $\frac{3}{2}\xi_c^2$) is small enough so that convergence can be achieved with a reasonable number of terms, this method would be the natural one to use.

For values of the exponent which are large compared to unity (in this case the lower limit ξ is of course the criterion), the following trick can be used.

Consider the integral $\int_L \frac{1}{x^2} e^{x^2} dx$, where L here (and from now on) designates the limits. This integral can be integrated by parts to yield

$$\int_L \frac{1}{x^2} e^{x^2} dx = -\frac{1}{x} e^{x^2} \Big|_L + 2 \int_L e^{x^2} dx .$$

Hence,

$$\int_L e^{x^2} dx = \frac{1}{2} \frac{1}{x} e^{x^2} \Big|_L + \frac{1}{2} \int_L \frac{1}{x^2} e^{x^2} dx . \qquad \text{(B-1)}$$

Similarly,

$$\int_L \frac{1}{x^4} e^{x^2} dx = -\frac{1}{3}\frac{1}{x^3} e^{x^2}\Big|_L + \frac{2}{3}\int_L \frac{1}{x^2} e^{x^2} dx$$

or

$$\int_L \frac{1}{x^2} e^{x^2} dx = \frac{3}{2}\int_L \frac{1}{x^4} e^{x^2} dx + \frac{1}{2}\frac{1}{x^3} e^{x^2}\Big|_L . \qquad \text{(B-2)}$$

Substituting (B-2) into (B-1) one obtains

$$\int_L e^{x^2} dx = \frac{1}{2}\frac{1}{x} e^{x^2}\Big|_L + \frac{1}{4}\frac{1}{x^3} e^{x^2}\Big|_L + \frac{3}{4}\int_L \frac{1}{x^4} e^{x^2} dx . \qquad \text{(B-3)}$$

In the next step one obtains

$$\int_L e^{x^2} dx = \frac{1}{2}\frac{1}{x} e^{x^2}\Big|_L + \frac{1}{4}\frac{1}{x^3} e^{x^2}\Big|_L + \frac{3}{8}\frac{1}{x^5} e^{x^2}\Big|_L + \frac{15}{8}\int_L \frac{1}{x^6} e^{x^2} dx .$$

(B-4)

This procedure can be continued as many times as necessary whereby each time the integrand of the remainder integral on the right hand side is decreased by the factor $\frac{1}{x^2}$. For $x >> 1$ the remainder integral becomes negligible compared with the integral on the left hand side after a few steps.

REFERENCES

Barasch, M. L. 1960. Report No. 2764-3-T. Radiation Laboratory, The University of Michigan.

Barasch, M. L. 1962. Report No. 3572-2-T. Radiation Laboratory, The University of Michigan.

Brown, S. C. 1959. Basic data of plasma physics (John Wiley and Sons, Inc., New York.

Dattner, A. 1957. Ericsson Techniques No. 2, Stockholm, p. 310.

Engel, A. von 1955. Ionized gases (Clarendon Press, Oxford)

Firsov, O.B. and Chibisov, M.I. 1961. Soviet Physics, JETP, 12, No. 6.

Golant et al. 1961. Soviet Physics, Tech. Phys. 6, 38 and 44.

Goodrich, R.F. et al. 1960. Report No. 3933-1-F. Radiation Laboratory, The University of Michigan

Hershberger, W.D. 1960. J. Appl. Phys. 31, No. 2.

Kamke, E. 1959. Differentialgleichungen Lösungsmethoden und Lösungen, Band 1. (Chelsea Publishing Co., New York).

Klopfenstein, R. W. 1954. IRE Trans., PGAP, AP-2, No. 3.

Langmuir, I. and Blodget, K. B. 1923. Phys. Rev. 22, 347.

Oster, L. 1961. Rev. Mod. Phys. 33, 525.

Ratcliffe, J.A. 1959. The magneto-ionic theory and its applications to the ionosphere (Cambridge at the University Press).

Romell, D. 1951. Nature 167, 243.

Schiff, L. 1949. Quantum mechanics, Eqn 35.23, p. 247, 1st edition (Mc-Graw Hill, New York).

Shkarovsky, I. P. 1961. Proc. IRE 49, 1857.

Tonks, L. 1931. Phys Rev. 37, 1458.